IRAQI BULLETIN OF GEOLOGY AND MINING (IBGM)\
IRAQ GEOLOGICAL SURVEY (GEOSURV-IRAQ)

*IBGM (**2025**, Vol 21; Issue 1)* *207-238*

LATERAL VARIATIONS IN THE RESERVOIR PROPERTIES OF THE MIDDLE MIOCENE JERIBE FORMATION IN THE ALLAS DOME OF THE HAMRIN OIL FIELD, NORTHERN IRAQ

Dler H. Baban[1*] and Muhamad B. M. Saeed[2]

[1] Department of Earth Sciences and Petroleum, Sulaimani University, Sulaimaniyah, Kurdistan Region-Iraq.
[2] Department of Earth Sciences and Petroleum, Sulaimani University, Sulaimaniyah, Kurdistan Region-Iraq; Directorate of Oil and Mineral in Sulaimaniyah, MNR, Kurdistan Region Government; e-mail: muhamadgeology@yahoo.com
***** *Corresponding author e-mail: dler.mohamad@univsul.edu.iq*

Type of the Paper (Article)
Received: 02/ 08/ 2024
Accepted: 04/ 02/ 2025
Available online: 27/ 06/ 2025

Abstract

The reservoir properties of the Jeribe Formation have been investigated from three wells in the southern dome of the Hamrin Oilfield (Allas Dome) based on conventional log data and cutting rock samples. The studied wells are arranged along the axis of the structure, which is in a southeast-northwest direction, with well Hr-50 being at the southeast part, followed by Hr-51 and Hr-49 towards the northwest. The Jeribe Formation's microfacies and wireline log analysis in the three wells located at the Allas Dome of the Hamrin Oilfield led to the conclusion that both lithology variations and fluid content within the formation's pore spaces are responsible for the variations in the recorded data of the wireline logs in well Hr-50 toward the northwest locations of wells Hr-51 and Hr-49. The Jeribe Formation's lithology at well HR-50 is mainly dolostone, with more prevalent grainstone microfacies. As it moves toward the other two wells, it becomes predominantly limestone, with increasing contents of wackestone and packstone microfacies. The formation in well HR-50 has an average shale content of roughly 18.2% and an average porosity of about 18.8%. In well HR-51, the average shale content and porosity are nearly 16.21% and 12.37%, respectively, while in well HR-49, the average shale content is about 18% and porosity about 12.73%. In well Hr-50, the distribution of the formation's shale is dispersed, laminated, and structural, whereas in the other two wells, dispersed shale distribution is nearly the only type that exists in the Jeribe Formation. The secondary porosity in the formation appears to be represented by separated voids, molds, and vugs, with well HR-50 exhibiting the largest percentage of secondary porosity (average 3.1%). The Jeribe Formation in wells Hr-51 and Hr-49 have predominantly gas reservoired hydrocarbons, while in well Hr-50 the formation is more likely to have oil reservoired hydrocarbons with a sizable immovable fraction. The three study wells' computed RQI and FZI values for the Jeribe Formation show that the formation has a tight reservoir rock type.

Keywords: Jeribe Formation; Hamrin Oilfield; Allas Dome; Reservoir properties; Log analysis.

ISSN 1811-4539, EISSN 3005-3714
https://doi.org/10.59150/ibgm2101a13
IBGM: http://ibgm-iq.org/
Academic Scientific Journals: www.iasj.net

1. Introduction

Iraq is one of the most actively researched countries in the world due to its quantity of petroleum. One of the giant oil fields in northern Iraq is Hamrin Oilfield, which, like most other Iraqi oil fields, has many pay zones.

The Paleogene-Neogene reservoirs, including part of the Transition Zone of the Fat'ha, Jeribe, Euphrates, and Kirkuk Group formations, and Cretaceous reservoirs, including Shiranish, Hartha, Sa'di, Khasib, Mishrif, Rumaila, Mauddud, Shu'aiba, and Yamama formations, are the main reservoirs found in the Hamrin Oilfield (INOC, 1994).

Within the Iraqi geological succession, the Middle Miocene Jeribe Formation is regarded as a major carbonate reservoir. Studies about this formation and characterizing its properties as a reservoir done by different authors in a lot of Northern Iraqi Oilfields [(Al-Ameri et al., 2011) (Ibrahim, 2008); (Fadhil, 2013); (Baban & Hussein, 2016); (Hussein et al., 2017); (Baban et al., 2018); (Alatroshe et al., 2018); (Abdulrahman et al., 2020); (Deabl et al., 2020); (Deabl et al., 2021); (Azeez et al., 2020); (AL-Sulaiman & Aadi Ahmed, 2021); (Hussein et al., 2022); (Gharib & Özkan, 2022); (Qader & Ali, 2022); (Baban et al., 2023); (Barzanji et al., 2023); (Akram et al., 2023); (Al-Jaff & Hamd-Allah, 2023); (Faidhllah & Hamd-Allah, 2023)].

This study aims to demonstrate the lateral variations in lithology, microfacies, and log responses of the Jeribe Formation across three selected wells on the Allas Dome of the field. The available data are adapted to follow the variations in the reservoir properties of the formation laterally, toward the northwest, from the location of well Hr-50 toward Hr-51 and Hr-49.

2. Hamrin Oilfield

The oilfield of Hamrin is located in northern Iraq, nearly 80 km southwest of Kirkuk City and 10 km north of Salahaddin Governorate (Figure 1A). The field is the SW anticlinal line of the Kirkuk block section of the Hamrin-Makul Subzone which is also known as Kirkuk-Hamrin, according to Aqrawi et al. (2010). It is structurally situated in the Zagros Low Folds Zone.

In terms of structure, Hamrin is made up of an asymmetrical longitudinal anticline with a northwest-southeast axis trend that is roughly 105 km long and 4.5 km wide, with a reflection on the surface (Figure 1A). Seismic data and field mapping revealed the existence of a sizable anticline that seems to be made up of three domes: Albofodhool, Nukhailah, and Allas, which are located from northwest to southeast. Ain Alnukhaila, which separates the Nukhailah and Albofodhool domes, and Darb Almilh, which separates Albofodhool and Allas domes, are the two known saddeles of the Hamrin structure (INOC, 1994). It is anticipated that a transverse fault would exist between the two saddles described, causing a displacement of roughly 450 meters between the beds on either side of the fault as mentioned in the report of the (INOC, 1994). The impact of the aforementioned transverse fault on the structural cross-section along the Allas and Nukhailah domes is depicted in Figure 1B.

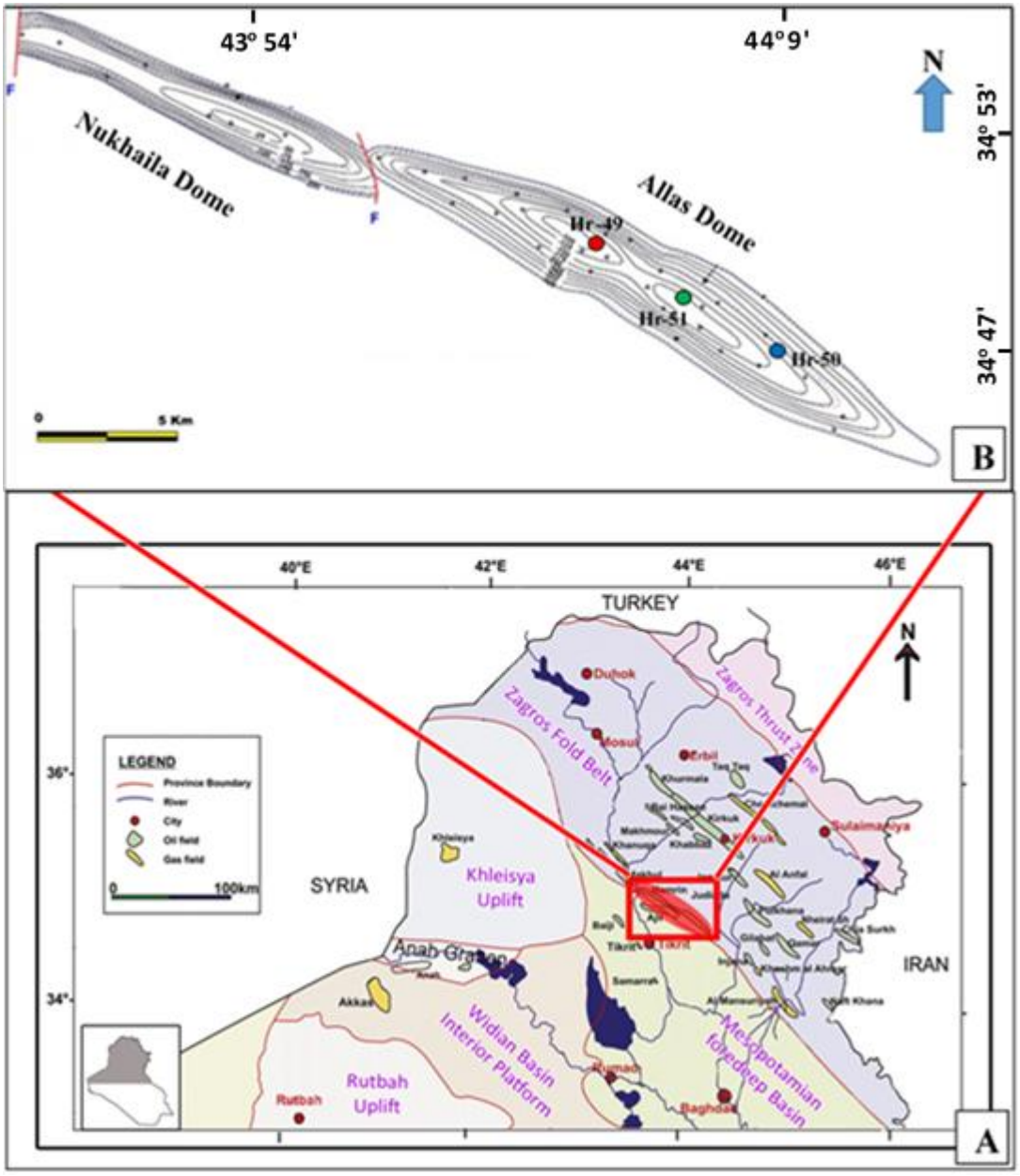

Figure 1. A) Location of the Hamrin Oilfield on a simplified tectonic map of Northern Iraq (after Al-Ameri & Zumberge, 2012 with a slight modification); B) locations of the studied wells on the structural map of Hamrin Oilfield (after INOC, 1994 in Mahdi, 2015).

3. Jeribe Formation

The Jeribe Formation is part of the greatest flooding surface Ng 20 (MFS 20) of the Arabian Plate Megasequence 11 (AP11) of Sharland et al. (2001). In the basin where it was deposited, the formation spread out somewhat evenly (Figure 2).

The Jeribe Formation represents a heterogeneous formation originally described as organic detrital limestone. In its type section, the Jeribe Formation comprises 70m of massive, recrystallized, and dolomitized limestones (Buday, 1980); (Jassim & Buday, 2006). Bellen et

al., (1959) state that the type section provides the majority of the facies' potential variations. Three primary facies that substantially interfinger with one another were mentioned. These include detrital, lithophyllide (reef), and lagoonal facies that were most likely deposited.

The Jeribe Formation, which is composed of limestone, dolomitic limestone, and dolostone, seemed to be around 50 meters thick in the wells under study. The lagoonal evaporitic beds of the Early Miocene Dhiban Formation underlie the formation, which is covered by the transition beds of the Middle Miocene Fat'ha Formation.

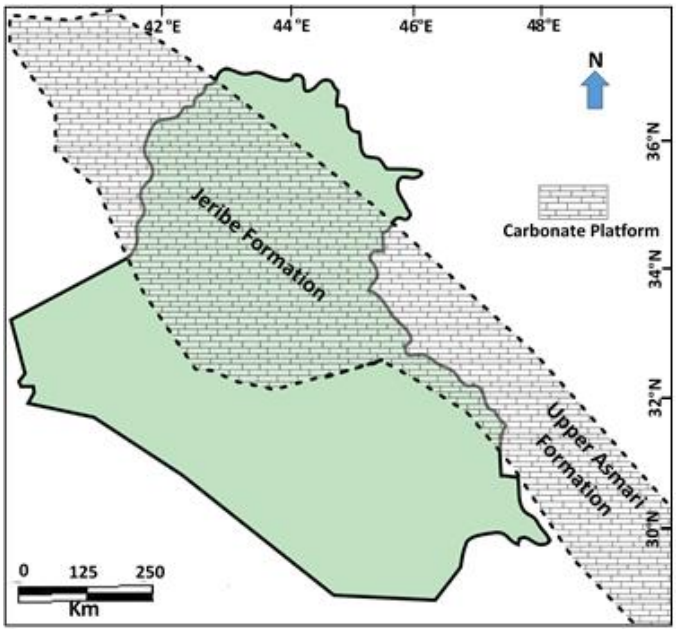

Figure 2. The basin setting in which the Jeribe Formation was deposited (modified after Aqrawi et al., 2010).

4. Results and Discussion

The lateral changes in the reservoir properties of the Jeribe Formation will be investigated in this study following the variations in the recorded wireline log data from the location of well Hr-50 toward the location of well Hr-49, which represents a lateral distance of about 8.3 km along the axis of the anticline from SE toward NW (Figure 1B).

4.1 Microfacies Analysis

Twenty-nine cutting rock samples were collected from the drilled Jeribe Formation in the three wells of the study for microfacies analysis, as shown in Table 1.

Table 1. The Jeribe Formation's thickness and depth intervals in the wells under study, together with the quantity of rock samples chosen from each well.

Wells	Elevation (m G.L.)	Jeribe Formation			Number of the cutting samples
		Thickness (m)	Top (m asl)	Bottom (m asl)	
Hr-50	307	51	213	264	13
Hr-51	321.09	49	150.5	199.5	8
Hr-49	308	47	106.5	153.5	8

Tables 2 – 4 are the details of the observed features through microscope examination of the studied rock samples selected from the wells of the study. The most noticeable variation is related to the lithology of the Jeribe Formation, which looks to be commonly dolostone in most of its parts in well Hr-50 in comparison to the formation's lithology in the other two wells of the study, in which limestone is dominant. The other important variation is the types of identified microfacies in well Hr-50, which contains more grainstone microfacies than the dominant wackestone and packstone microfacies in the other two wells.

Table 2. Common lithology, pore types, microfacies, and diagenesis characteristics were found in the Jeribe Formation under study in well HR-50.

Sample Depth (m)	Common lithology	Microfacies Type	Pore types	Diagenesis
527	Dolostone, Limedolostone	Wackestone/ Packstone	Intercrystalline, interparticle, intraparticle	Cementation, dolomitization
528	Dolostone, Limedolostone	Wackestone/ Packstone	Intercrystalline, intraparticle, moldic,	Cementation, dissolution, dolomitization pyritization
530	Dolomitic limestone	Wackestone/ Packstone	Intercrystalline, intraparticle, interparticle, moldic,	Cementation, dissolution, dolomitization
533	Argillaceous dolostone	Packstone/ Grainstone	Intraparticle, interparticle, moldic,	Cementation, dissolution
535	Argillaceous dolostone	Foraminifera Bearing Packstone	Microfractures, vugs, intercrystalline	Cementation, dissolution, fracturing
537	Argillaceous dolostone	Grainstone/ Packstone	Intercrystalline, Intraparticle, vugs, interparticle, moldic,	Cementation, dissolution, pyritization
539	Argillaceous dolostone	Grainstone/ Packstone	Intercrystalline, intraparticle, interparticle, moldic, vugs	Cementation, dissolution
542	Argillaceous dolostone	Foraminifera Bearing Grainstone	Intraparticle, interparticle, moldic, shelter, vugs	Cementation, dissolution
544	Dolostone with Anhydrite nodules	Packstone/ Wackstone	Intercrystalline, microfractures, vugs	Cementation, dissolution, fracturing, dolomitization
548	Limestone	Foraminifera Bearing Grainstone/ Packstone	Interparticle, intraparticle, channel, shelter	Cementation, dolomitization
550	Dolostone, limedolostone	Packstone/ Wackstone	Intercrystalline, interparticle, intraparticle	Cementation, dolomitization
564	Calcareous dolostone	Grainstone/ Packstone	Intercrystalline, intraparticle, interparticle, moldic	Dissolution, cementation
568	Dolostone, limedolostone	Calcite crystal bearing Wackestone	Intercrystalline, vugs	Dissolution, cementation, dolomitization
570	lime dolostone	Packstone/ Grainstone	Intercrystalline, shelter, moldic, vugs	Dissolution, cementation, dolomitization

Table 3. Common lithology, pore types, microfacies, and diagenesis characteristics were found in the Jeribe Formation under study in well HR-51.

Sample Depth (m)	Common lithology	Microfacies Type	Pore types	Diagenesis
478	Limestone	Wackestone	Vugs	Dissolution
486	Argillaceous limestone	Wackestone	Vugs	Dissolution
494	Argillaceous limestone	Algal bearing Packstone	interparticle, intraparticle	Dissolution, cementation, pyritization
502	Limestone	Wackestone/ Packstone	Vugs, microfractures, interparticle, intraparticle	Dissolution, cementation, fracturing
510	Limestone	Wackstone/ Packstone	Vugs, interparticle, intraparticle	Dissolution, cementation
520	Limestone	Wackestone/ Packstone	Vugs, interparticle, intraparticle	Dissolution, cementation

Table 4. Common lithology, pore types, microfacies, and diagenesis characteristics were found in the Jeribe Formation under study in well HR-49.

Sample Depth (m)	Common lithology	Microfacies Type	Pore types	Diagenesis
420	Limestone	Wackestone	Intraparticle, moldic	Cementation, dissolution
422	Limestone	Foraminifera Bearing Packstone	Interparticle, intraparticle	Cementation
426	Limestone	Foraminifera Bearing Packstone	Intraparticle, shelter	Cementation
432	Argillaceous Limestone	Packstone/ Grainstone	Interparticle, microfractures, intraparticle, moldic	Cementation, fracturing, dissolution
436	Argillaceous limestone	Algal Bearing Wackestone	Microfractures, vugs	Cementation, dissolution, fracturing
452	Limestone	Foraminifera Bearing Packstone	Microfractures, vugs, interaparticles, interparticles	Cementation, dissolution, dolomitization, fracturing
456	Limestone	Wackestone/ Packstone	Intraparticle, moldic, vugs	Dissolution
464	Dolomitic limestone	Wackestone/ Packstone	Intraparticle, moldic, vugs	Cementation, dissolution, dolomitization
466	Limestone	Wackestone/ Packstone	Intraparticle, interparticle, vugs	Cementation, dissolution

Dolostone being the common lithology of the Jeribe Formation in well Hr-50, the intercrystalline type of porosity, as expected, was observed to be the dominant pore type available in the formation besides other interparticles, intraparticles, molds, and vugs, which were generally common in the three wells of study especially wells Hr-50 and Hr-49. Primarily, from the two-dimensional thin section examination, the vugs and the molds looked like separated open or partially open pores; there was no way to be sure about the possibility of their connections in the three-dimensional case of the rock. Fractures also looked to exist as a secondary porosity type, but it was less common.

Different kinds of destructive and constructive porosity diagenesis processes were observed in the examined thin sections. Dissolution was the most common constructive diageneses that affected the Jeribe Formation, from which a lot of vug- and mold-type porosity was produced. On the other hand, cementation was the most effective diagenesis that negatively affected the porosity of the Jeribe Formation. Dolomitization was obvious in well Hr-50 and was less intense in the other two wells. Figure 3A – 3L in Plate 1 are examples of the different microfacies identified in the Jeribe Formation in the wells of the study, along with examples of the types of primary and secondary porosities observed in the examined thin sections at different depths.

4.2. Lithology Determination from Log Data

The neutron log measures the amount of hydrogen in formation, which is thought to be connected to fluids invading pore spaces within the reservoir rock, On the other hand, the density log measures the electron density, and from that formation bulk density, lithology can be ascertained (Asquith & Krygowski, 2004).

Applying this method in the current study (Figure 4), the lithology of the Jeribe Formation in well Hr-50 showed an obvious dolostone, whereas in well Hr-51 (Figure 4B), the sample points distorted more toward the limestone line, indicating dominant dolomitic limestone and limestone lithology. In well Hr-49, the sample points showed exaggeration in distortion towards the limestone and even the sandstone line as an indication of the less dolomitic nature of the Jeribe Formation's lithology. As the nature of the enclosed fluids in the rock pore spaces as water, oil, or gas affects the responses of the density and neutron logs, thus the distortion of sample points toward the sandstone line and upper may be due to variations in the reservoired fluids in the Jeribe Formation at the location of the Hr-50 and the other two wells of Hr-51 and Hr-49. It's more likely that the Jeribe Formation in well Hr-50 contains oil, whereas the other two wells contain more gas, especially in well Hr-49.

Another method is the M-N plot, which combines the three porosity measurements (sonic, density, and neutron) so that two values can be utilized in a cross-plot to display the lithology (Asquith & Krygowski, 2004). The two calculated values, known as M and N, are calculated by applying Equations 1 and 2. Figures 5 – 7 show the distribution of the sample points on the M-N diagram for the Jeribe Formation in the three wells of the study.

$$M = \left(\frac{\Delta tfl - \Delta t}{\rho b - \rho fl}\right) * 0.01 \quad (1)$$

$$N = \left(\frac{\emptyset Nfl - \emptyset N}{\rho b - \rho fl}\right) \quad (2)$$

Where: Δt = the recorded interval transit time in the formation by the sonic log. Δtfl = interval transit time in the fluid in the formation. ρb = the recorded formation bulk density by the density log. ρfl = fluid density. ØN = the recorded neutron porosity. ØNfl = neutron porosity of the formation fluid (usually= 1.0).

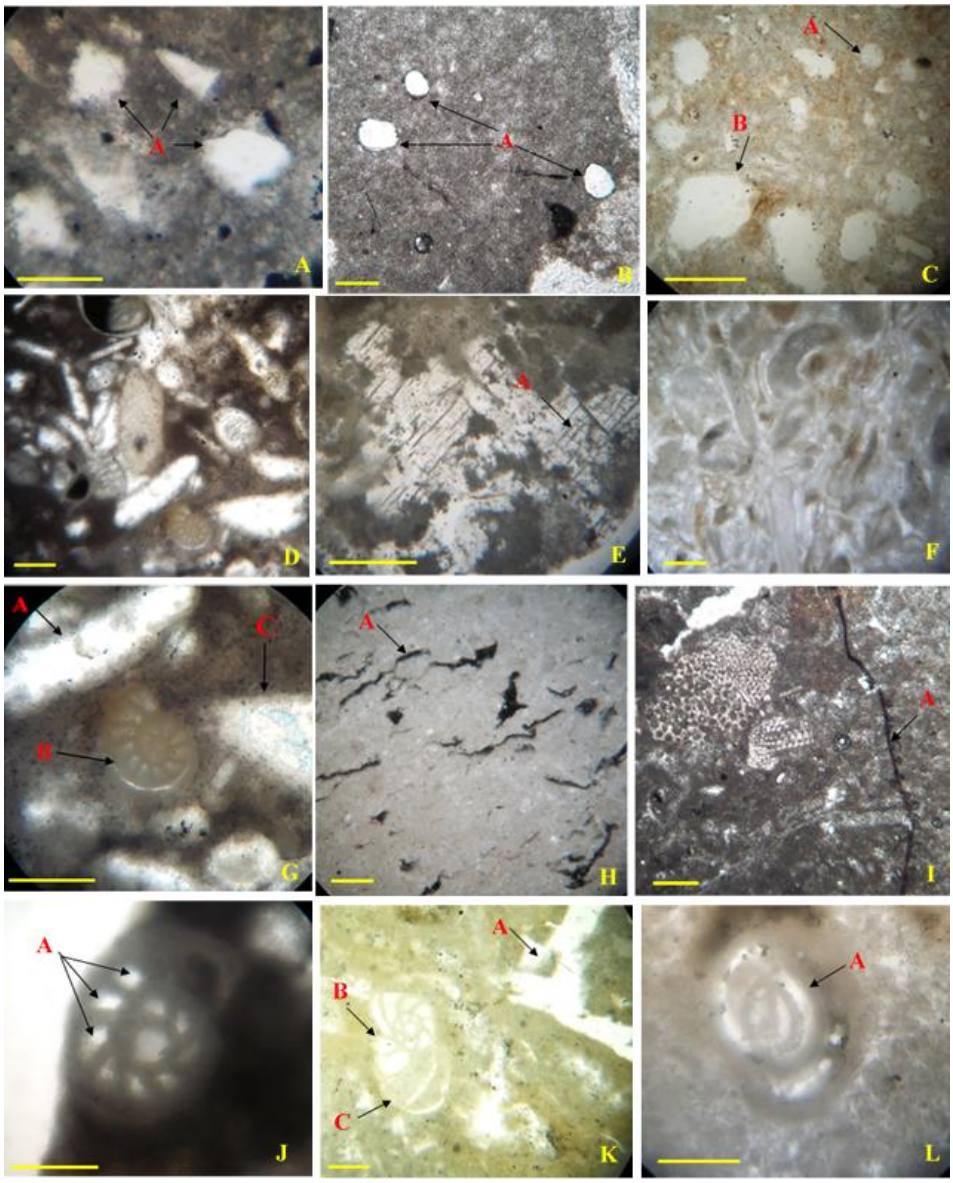

Figure 3: (The bar scale on the photomicrographs is equal to 100 µm).
A) Packstone/ Grainstone Microfacies, A: moldic porosity, B: shelter porosity, C: cement filled vug, Depth: 570 m, well Hr-50. B) Wackestone/ Packstone Microfacies, A: separated vugs, Depth: 520 m, well Hr-51. C) Wackestone/ Packstone Microfacies, A: moldic porosity, B: separated vugs, Depth: 464 m, well Hr-49. D) Packstone/ Grainstone Microfacies, Depth: 570 m, well Hr-50. E) Foraminifera bearing Packstone Microfacies, A: two sets of fractures, Depth: 452 m, well Hr-49. F) Foraminifera bearing Grainstone Microfacies, Depth: 542 m, well Hr-50. G) Packstone/ Grainstone Microfacies, A: moldic porosity, B: shelter porosity, C: cement filled vug, Depth: 570 m, well Hr-50. H) Algal bearing Wackestone Microfacies, A: bitumen filled fractures, Depth: 436 m, well Hr-49. I) Algal bearing Packstone Microfacies, A: bitumen filled microfracture, Depth: 494 m, well Hr- 51. J) Foraminifera bearing Packstone Microfacies, A: intraparticle porosity, Depth: 422 m, well Hr-49. K) Foraminifera bearing Grainstone/ Packstone Microfacies, A: channel porosity, B: Intraparticle porosity, C: interparticle porosity, Depth: 548 m, well Hr-50. L) Foraminifera bearing Packstone Microfacies, A: intraparticle porosity, Depth: 422 m, well Hr-49.

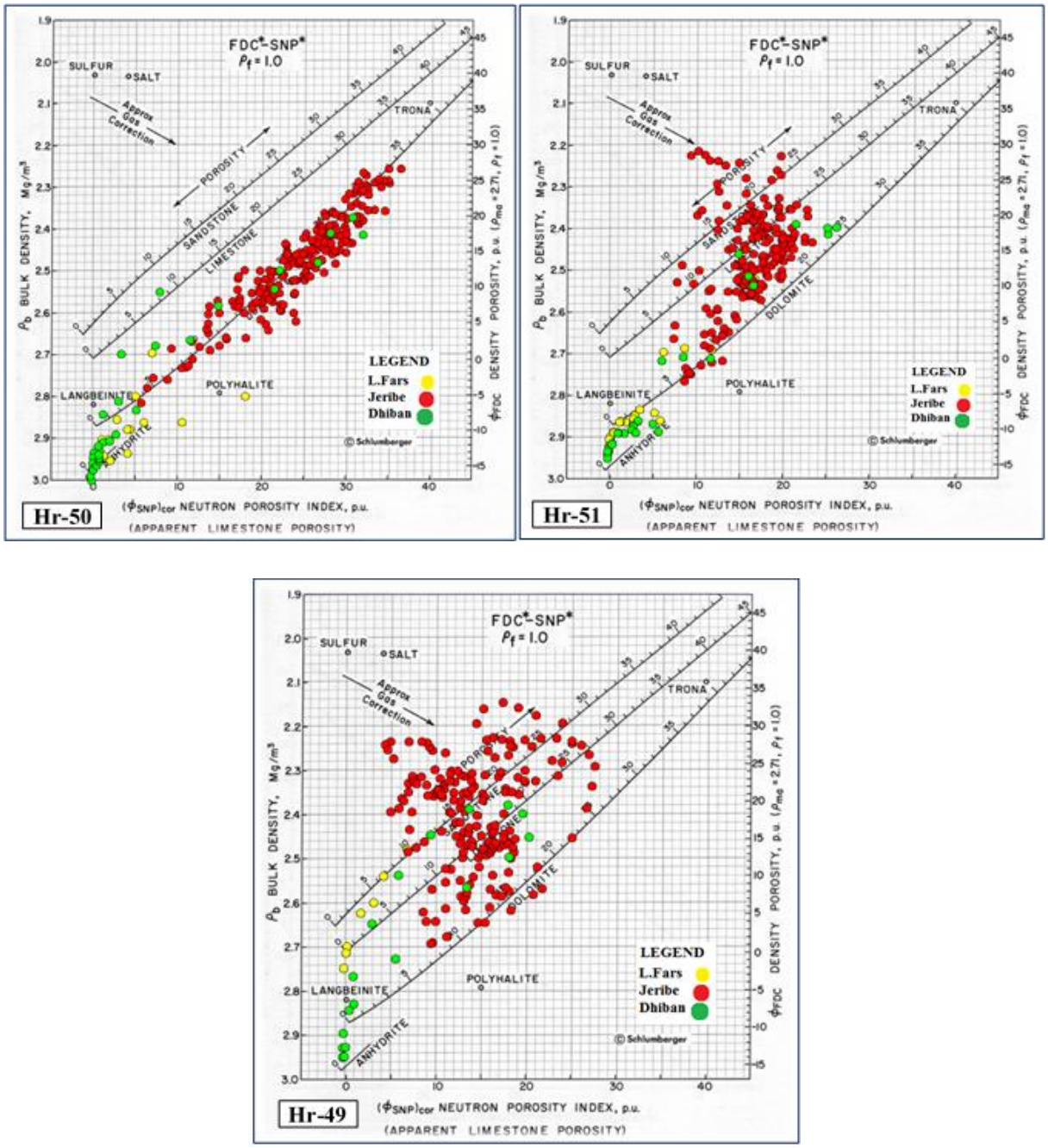

Figure 4. Density versus neutron crossplot for determining lithology of the Jeribe Formation in the studied wells. Additionally, the lithology of the Dhiban and Fat'ha formations was also identified (the crossplot is based on Schlumberger, 1989).

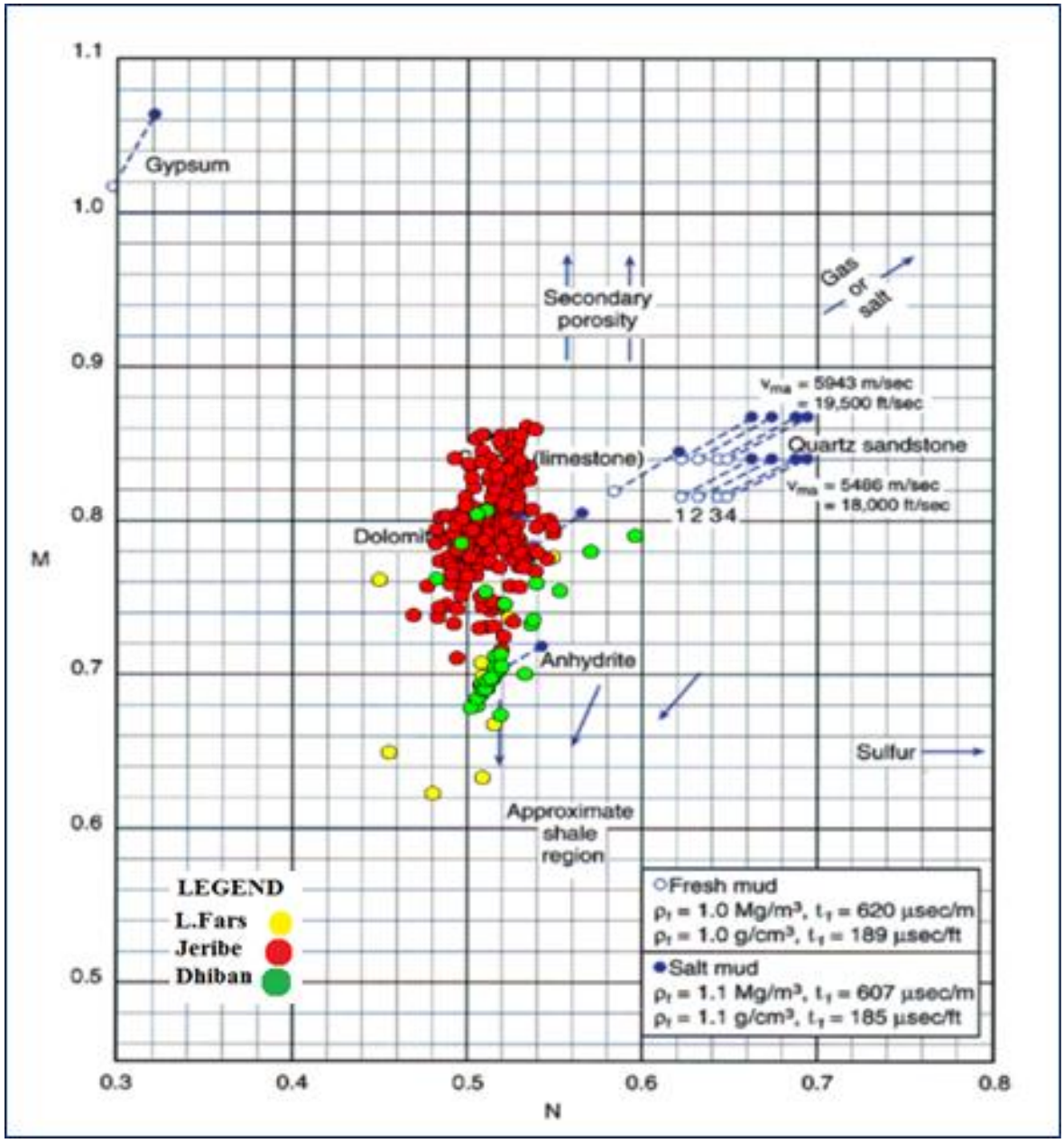

Figure 5. M-N crossplot to identify the lithology of the Jeribe Formation under study in well HR-50. Additionally, the lithology of the Fat'ha and Dhiban formations was determined (the crossplot was based on Schlumberger, 1989).

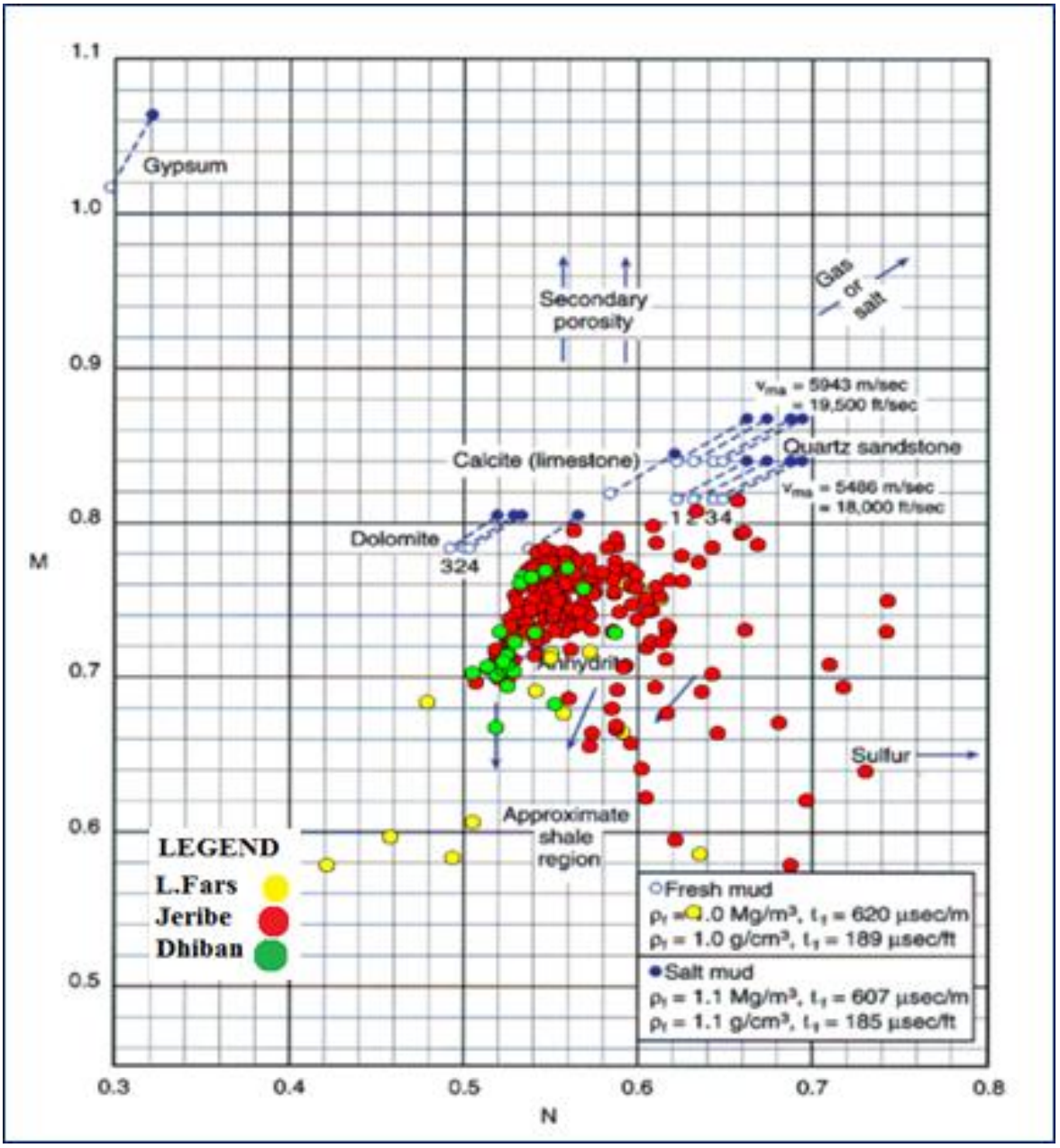

Figure 6. M-N crossplot to identify the lithology of the Jeribe Formation under study in well HR-51. Additionally, the lithology of the Fat'ha and Dhiban formations was determined (the crossplot was based on Schlumberger, 1989).

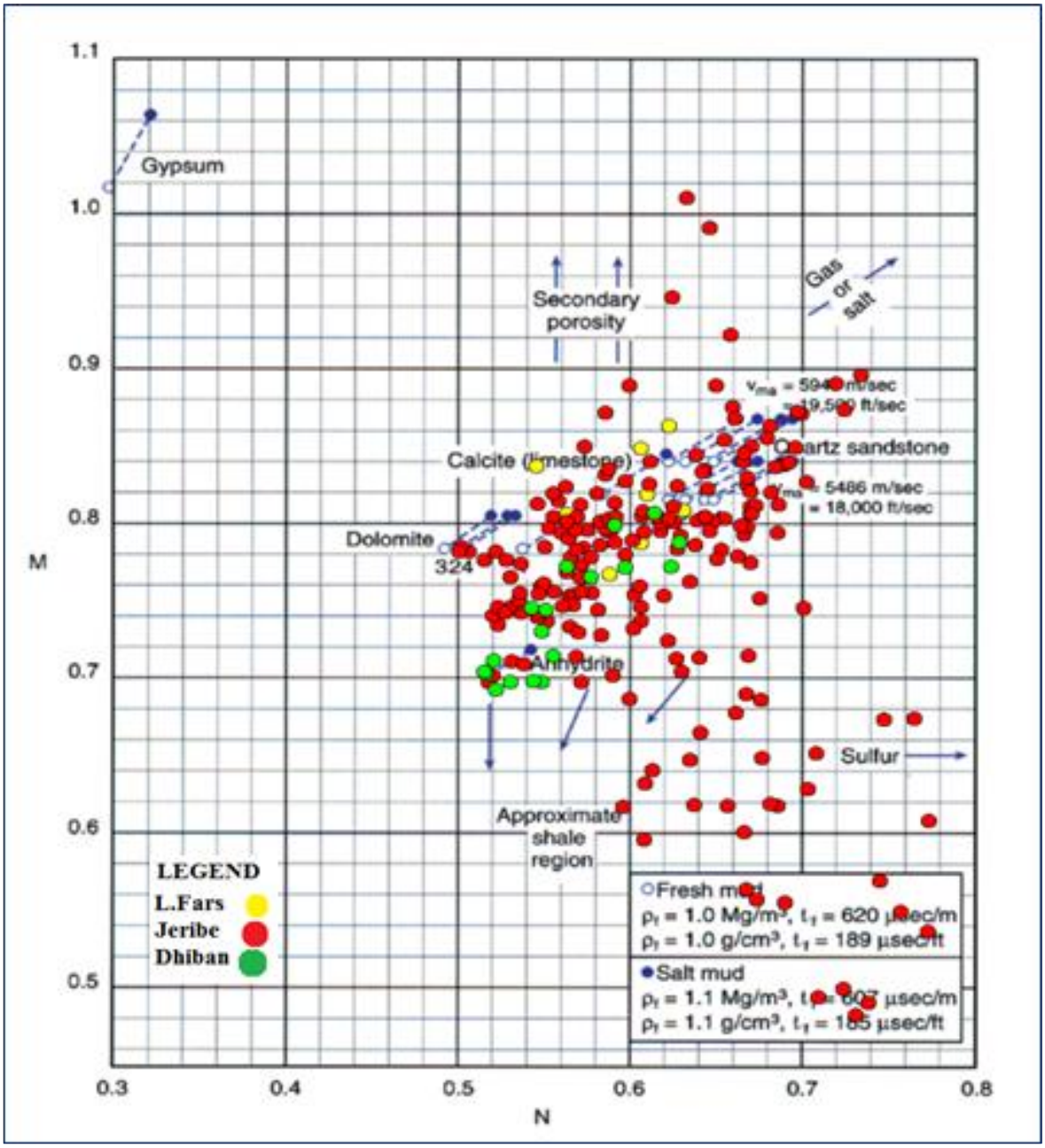

Figure 7. M-N crossplot to identify the lithology of the Jeribe Formation under study in well HR-49. Additionally, the lithology of the Fat'ha and Dhiban formations was determined (the crossplot was based on Schlumberger, 1989).

The concentration of the sample points around the dolomite can clearly be noticed in well Hr-50, with more and more scattering of the sample points toward wells Hr-51 and Hr-49. The scatter of the sample points toward the limestone as a lithology, also toward the gas region, and partially toward the shale region. The Jeribe Formation in the location of well Hr-49 looks to have the highest ratio of shale and the least is in the location of well Hr-50.

4.3. Shale Content

Shale volume for the Jeribe Formation has been computed from the data of the gamma-ray log using the standard procedure for determining the gamma-ray index (GRI) (Equation 3) and then applying the (Larionov, 1969) equation for unconsolidated Tertiary beds (Equation 4).

$$GRI = \frac{\text{GRlog} - \text{GRmin}}{GRmax - GRmin} \tag{3}$$

$$Vsh = 0.83[2^{(3.7*GRI)} - 1.0] \tag{4}$$

Where: GRI = Gamma-ray index; GR_{log} = Gamma-ray reading from log; GR_{min} = Minimum gamma ray reading from log (clean zone); GR_{max} = Maximum gamma ray reading from log (shale zone); Vsh = Volume of shale.

Figure 8 shows the calculated shale volume for the Jeribe Formation in the wells of the study. Clean, shaly, and shale zones were identified based on (Ghorab et al., 2008) suggestion for zones containing less than 10% shale, between 10 and 35%, and zones of greater than 35% shale content, respectively.

The Jeribe Formation at the three studied wells looks to have higher percentages of shale content at its middle part, being relatively highest in well Hr-49. In well Hr-50, the shaly zone of the formation is of wider thickness than the other two wells of Hr-51 and Hr-49 (Table 5). Such variations in shale content are mostly related to the paleo-depositional situation.

Regarding modes of shale distribution within the Jeribe Formation, variations were also detected between the locations of the selected wells for the study. The variety of effects that shale content in reservoirs can have, as well as the severity of those effects, depends on the volume, nature, and distribution of shale in the reservoir rock. When assessing formations and carrying out drilling operations, shale also poses substantial obstacles (Baban et al., 2023).

Based on the proposed relationship between ØD and ØN by Thomas & Stieber (1975) for determining the modes by which shales may distribute in sandstone reservoir rocks and applying the same method in carbonate reservoir rocks (Yang, 2015); (Moradi et al., 2016); (Baban et al., 2020); (Baban & Ahmed, 2022), types of shale distribution were identified in the Jeribe Formation in wells of the study (Figure 9).

The shale in the Jeribe Formation in well Hr-50 is distributed in almost three known modes dispersed, laminated, and structural, with the dispersed mode being the dominant. In contrast to wells Hr-51 and Hr-49, no gas effect was detected in the Jeribe Formation in well Hr-50.

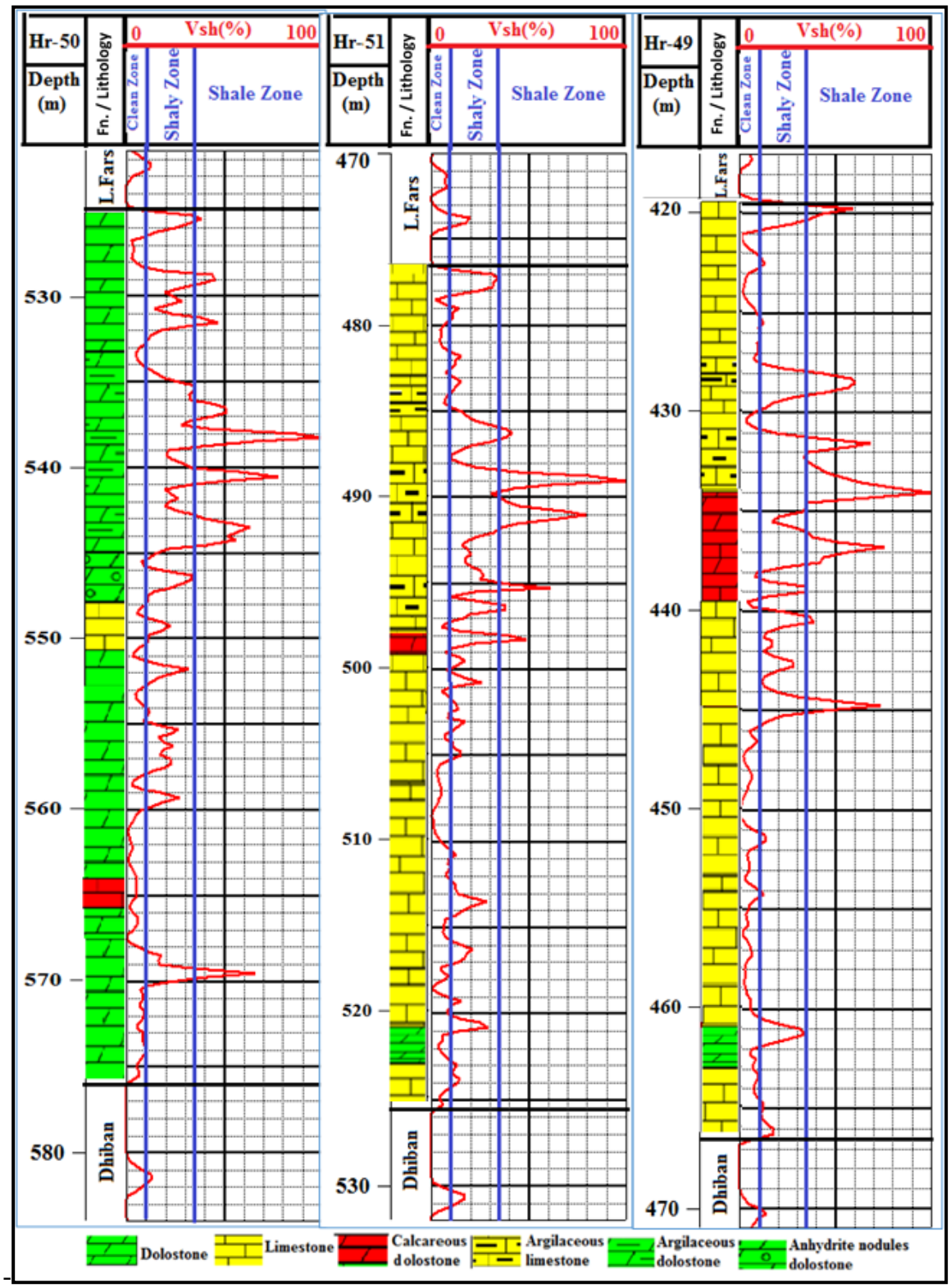

Figure 8: Shale volume and shale content zonation curve graphs along the wells under study (Hr-49, Hr-50, and Hr-51).

Table 5. The average shale content and the standard suggested by Ghorab et al. (2008) as used to determine the clean, shaly, and shale zones in the study's wells.

Wells	Zone	Interval (m)
Hr-50	Shaly zone	525.00 – 535.00
	Shale zone	535.00 – 545.00
	Shaly zone	545.00 – 560.00
	Clean zone	560.00 – 576.00
Hr-51	Clean zone	476.50 – 488.00
	Shale zone	488.00 – 493.00
	Shaly zone	493.00 – 501.00
	Clean zone	501.00 – 525.50
Hr-49	Clean zone	419.50 – 428.00
	Shale zone	428.00 – 438.00
	Shaly zone	438.00 – 445.00
	Clean zone	445.00 – 466.50

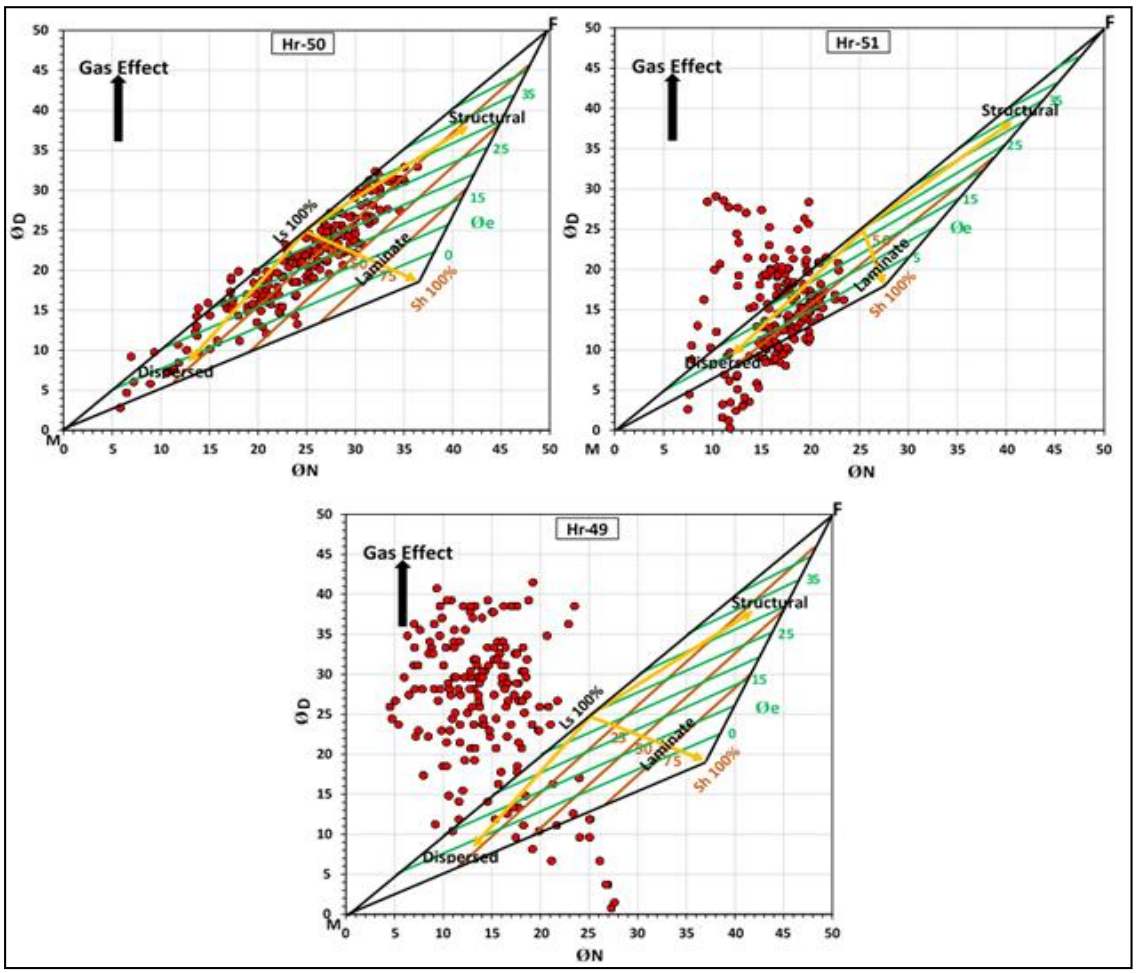

Figure 9. Modes of shale distribution in the Jeribe Formation in wells Hr-50, Hr-51, and Hr-49.

Ignoring the gas effect in the diagrams of shale distribution for wells Hr-51 and Hr-49 (Figure 9), the dispersed type of shale distribution is almost the only way by which the clay minerals are distributed between the grains of the Jeribe reservoir rocks. It's important to mention that reservoir zones with structural shale distribution won't see a decrease in porosity and permeability as a result of the shale content since each of the three forms of shale distribution has a different effect on these properties. Zones where the shale component is distributed among the grains (dispersed) have the greatest loss in reservoir parameters (taking into consideration the type of clay minerals forming the shale) (Tiab & Donaldson, 2012); (Ellis & Singer, 2007).

Clay minerals, which make up dispersed shale, are produced by chemical reactions between minerals in the formation of water and minerals themselves because of a variety of crystal sizes and shapes (Saxena et al., 2006). Sequential repetition of laminated shale is caused by deposition under two different flow regimes that are taken into account by energy differences (Visser, 1998) lasts of structural shale are deposited during the early depositional stage (Kurniawan & Kurniawan, 1996). Thus, variation in the paleodepositional environment of the Jeribe Formation at the location of well Hr-50 from the locations of the other two wells is expected.

4.4. Porosity Calculations

For the Jeribe Formation, the porosity based on information from the conventional porosity logs of sonic, density, and neutron, in the study wells has been computed. The values of the porosity have been corrected from the shale impact which usually causes an unreal increase of the porosity for the logged interval.

The corrected combination neutron-density porosity ($Ø_{ND}$) for the Jeribe Formation was calculated and plotted as shown in Figure 10 along with the calculated shale content to show the reduction in the porosity values, which is proportionally related to the shale volume.

As a general trend line, the porosity of the Jeribe Formation has almost the same increase and decrease trend along the three studied sections with a relatively higher porosity value in the formation in well Hr-50. The average corrected ØND of the formation is 18.8%, 12.37%, and 12.73% for wells Hr-50, Hr-51, and Hr-49, respectively. The lowest porosity values were observed to be in the middle part of the formation, where the relatively highest shale content exists.

It's important to mention that although the Jeribe Formation in well Hr-50 showed an average shale content of about 18.2%, but still the formation in this well of higher average porosity than the other two wells of Hr-51 and Hr-49 shale content are 16.21%, and 18%, respectively. This is most likely due to the mode of the shale distribution in the Jeribe Formation in well Hr-50, which appeared to be partly of laminated and structural types, which, in contrast to the dispersed shale distribution type, both have less or no effect on the porosity and permeability (Ellis & Singer, 2007; Tiab & Donaldson, 2012).

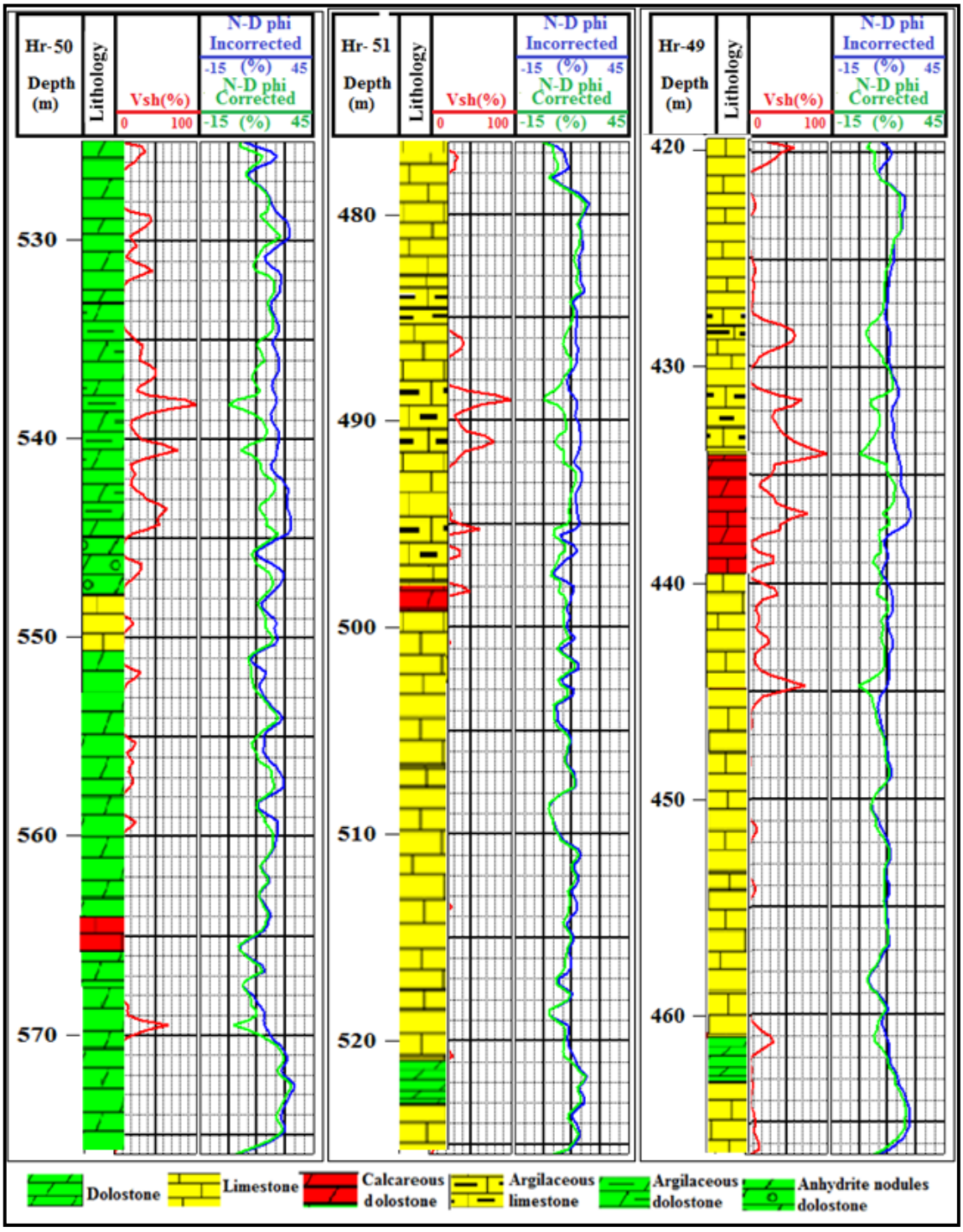

Figure 10. Shale volume curves and the corrected and uncorrected N-D porosity from the shale effect for the Jeribe Formation under study in wells Hr-50, Hr-51, and Hr-49.

The data of the calculated density porosity ($Ø_D$) and neutron porosity ($Ø_N$) after correction from the shale effect were adapted as crossover curves (Figure 11) to detect the nature of the reservoired fluids within the pore spaces of the Jeribe Formation. As gas, compared to oil and water, has a lower electron number and lower hydrogen content, gas-bearing zones are expected

to have low ØN values and high ØD values. Accordingly, the Jeribe Formation in wells Hr-51 and Hr-49 looks to contain mainly gas rather than oil, whereas the formation in well Hr-50 is most likely to bear oil except in those zones where the porosity is too low and hens of high capillary pressure where the trapped gases cannot easily be displaced by the invaded oils.

Moreover, the gas effect is best detected by the matrix identification (MID) cross plot using apparent matrix density (ρma)a versus apparent matrix travel time (Δtma)a as shown in Figure 12.

$$(\rho m)a = \left(\frac{\rho b - \emptyset ND * \rho fl)}{(1 - \theta ND)}\right) \quad (5)$$

$$(\Delta tma)a = \left(\frac{\Delta t - \emptyset SN * \Delta tfl}{1 - \emptyset SN)}\right) \quad (6)$$

Where: (ρma)a = apparent grain density in g/cm³; (Δtma)a = apparent matrix interval transit time in μsec/ft; ρb = bulk density from the density log; ρ_{fl} = fluid density; Δt = interval transit time from the sonic log; Δt_{fl} = interval transit time of fluid; $Ø_{ND}$ = combination neutron-density porosity; $Ø_{SN}$ = combination sonic-neutron porosity.

The gas effect in the Jeribe Formation is very obvious in wells Hr-51 and Hr-49, with no detection of such an effect in well Hr-50. It can also be observed that the gas effect is highest in well Hr-49, and that is mostly due to the location of the well closest to the crest of the Allas Dome.

For investigating the existence of secondary (fracture) porosities in the Jeribe Formation in wells of the study, the technique of subtracting sonic porosity from density, neutron, or combination neutron-density porosity is applied.

It's well known that the calculated sonic porosity ($Ø_S$) represents the matrix (primary) porosity of the rock, whereas the calculated density porosity and the recorded neutron porosity represent the total (primary and secondary) porosity of the rock (Asquith & Gibson, 2004); (Rider, 2002); (Asquith & Krygowski, 2004).

Figure 13 is the calculated secondary porosity for the Jeribe Formation in the wells of the study. The formation in well Hr-50 showed the highest average secondary porosity (3.1%), and the lowest average secondary porosity in well Hr-51 (0.58%), whereas in well Hr-49 the average secondary porosity appeared to be 2.78%.

Although the calculated secondary porosity in this way is sometimes called fracture porosity, it doesn't necessarily represent fractures because voids, vugs, and large molds may also coexist as secondary porosities that are not sensed by the sonic logging tool.

As the calculated secondary porosity in the Jeribe Formation in well Hr-50 is the highest and

there is no gradual increase toward locations of wells Hr-51 and Hr-49 (which both are closer to the crest of the Allas Dome), it's more likely for those secondary porosities to be voids, vugs, or even large molds than fractures.

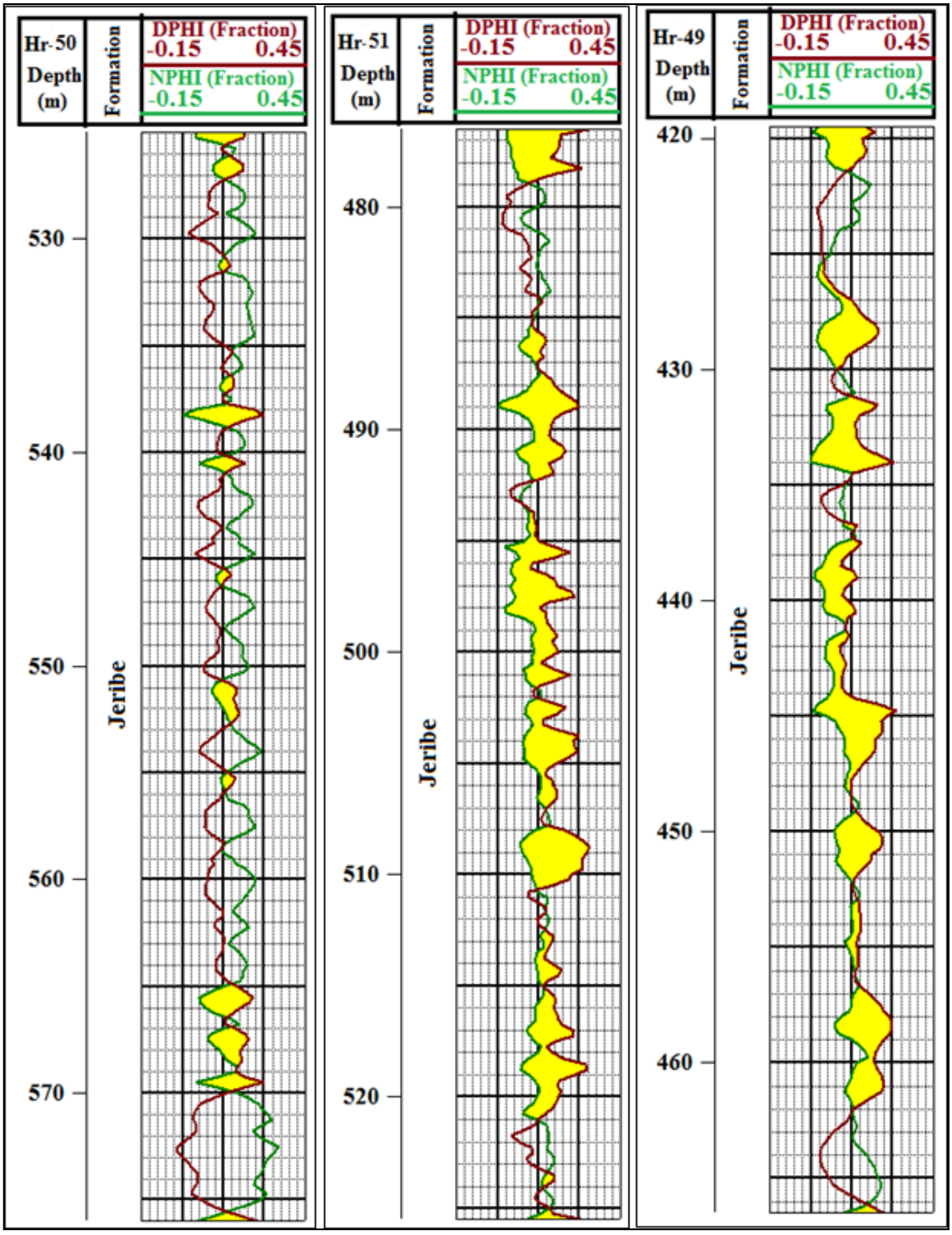

Figure 11. Neutron and Density porosity curve's crossovers for detecting gas-bearing zones in the studied Jeribe Formation in each of Hr-50, Hr-51, and Hr-49 wells.

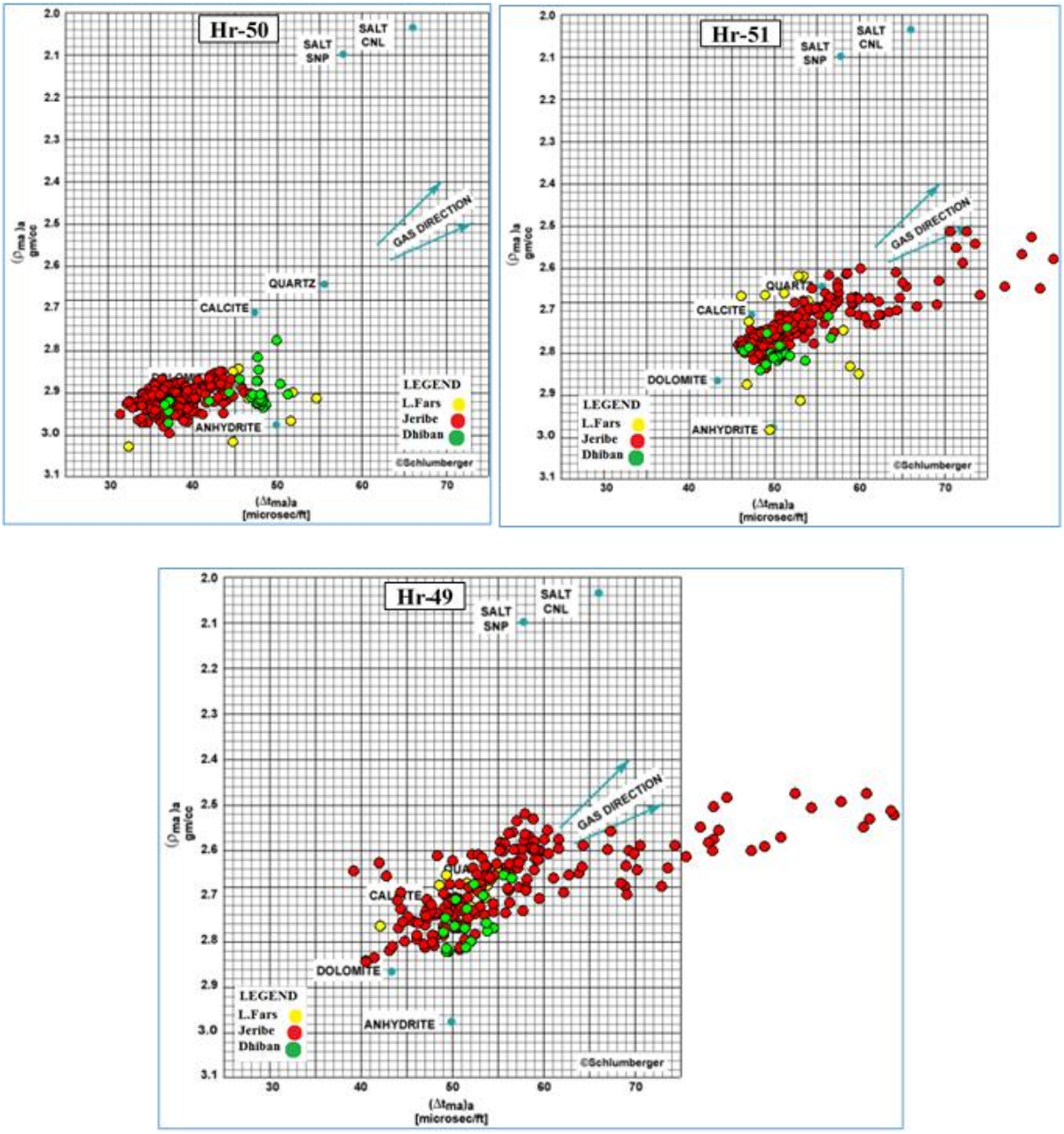

Figure 12. MID plot for lithology identification for Jeribe Formation in the studied wells. The lithology of the Dhiban and Fat'ha formations was also identified (the crossplot is after (Schlumberger, 1972).

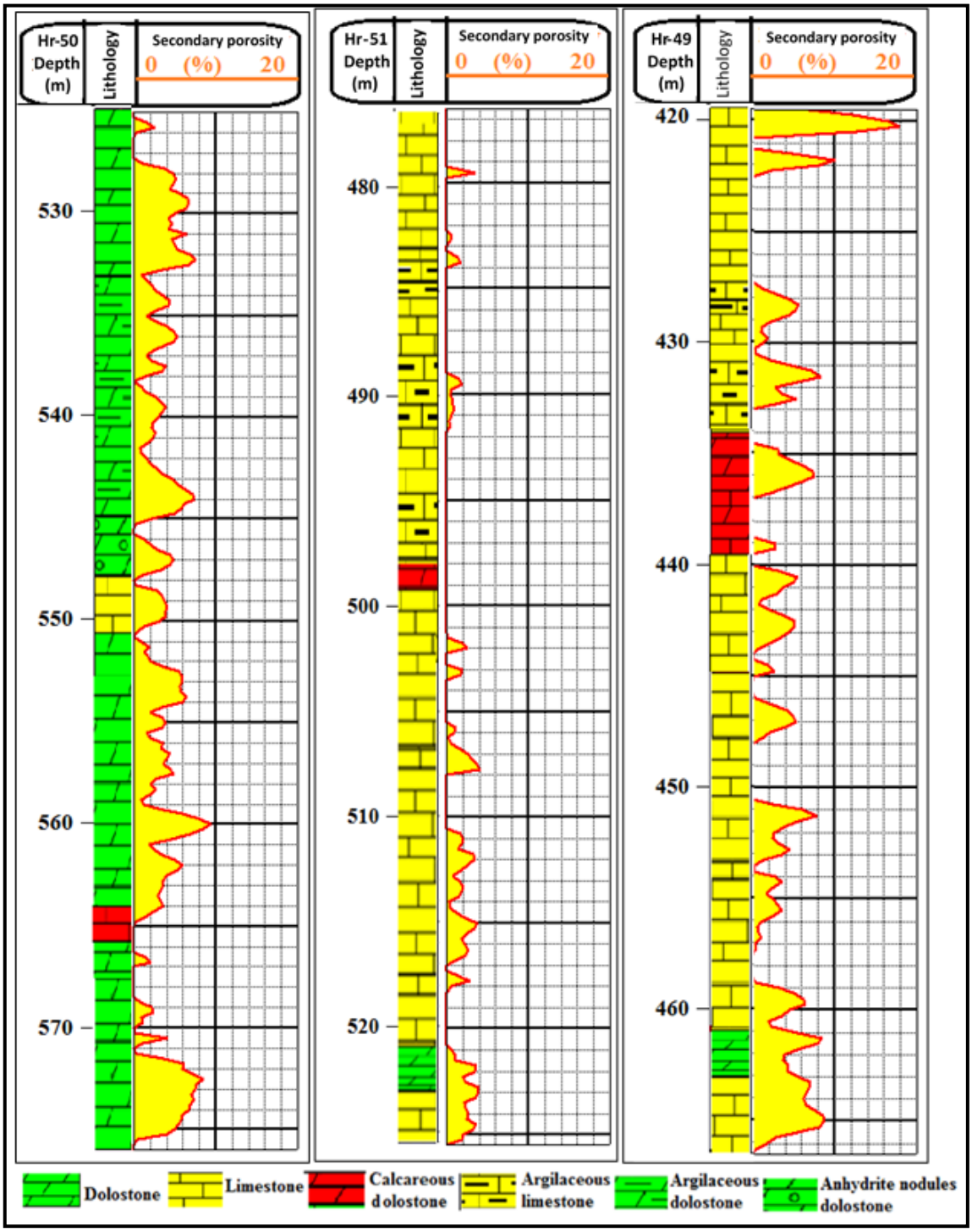

Figure 13. Secondary porosity plot for the studied Jeribe Formation in wells Hr-50, Hr-51, and Hr-49.

4.5. Water and Hydrocarbon Saturations

Because they can consistently and affordably offer information regarding the resistivity (reciprocal conductivity) of the penetrated formation, electrical logs are regarded as crucial tools for measuring water and hydrocarbon saturation.

The conductivity of any reservoir rock results from the constant presence of hydrocarbons and/or water in the pore space. The amount of water present and the conductivity of the water in the pores will determine the actual conductivity.

Conductivity is also influenced, albeit to a lesser degree, by the lithology of the rock matrix, the amount of clay in it, and its texture, which includes the distribution of pores, conductive minerals, and grain size. It's crucial to note that temperature has a significant impact on a reservoir bed's conductivity (Ellis & Singer, 2007).

Archie equations, Equations 7 and 8, are the most popular equations used for calculating water saturation from log data for the uninvaded zone and the flushed zone, respectively.

$$w = (F * \frac{Rw}{Rt})^{1/n} \quad (7)$$

$$Sxo = (F * \frac{Rmf}{Rxo})^{1/n} \quad (8)$$

Where: Sw: Water saturation in the uninvaded zone; a: Tourtasity factor (generally equal to 1.0); m: Cementation exponent; Ø: Porosity; Rw: Formation water resistivity (Ω.m); Rt: True resistivity (Ω.m); Sxo: Water saturation in the flushed zone; Rmf: Resistivity of the mud filterate (Ω.m); Rxo: Resistivity of the flushed zone (Ω.m); n: Saturation exponent (its value ranges from 1.8 to 2.5 but mostly equal to the value 2.0).

From the calculated water saturations for the uninvaded and flushed zones, residual (Shr) and movable hydrocarbon saturations (Shm) were calculated applying Eq. 9 and Eq. 10 equations, respectively, and plotted as shown in Figure 14.

$$Shr = 1 - Sxo \quad (9)$$

$$Shm = 1 - Sw - Shr \quad (10)$$

The Jeribe Formation in the three studied wells looks to contain hydrocarbons along its thickness in different saturation percentages. In addition to the variation in porosity between well Hr-50 and wells Hr-51 and Hr-49, the hydrocarbon also looks to have a higher saturation percentage in well Hr-50 compared to the other two wells.

Noticeable is the high percentage of residual (immoveable) hydrocarbon saturation in the Jeribe Formation in well Hr-50, which might be due to the nature of the hydrocarbons in this well.

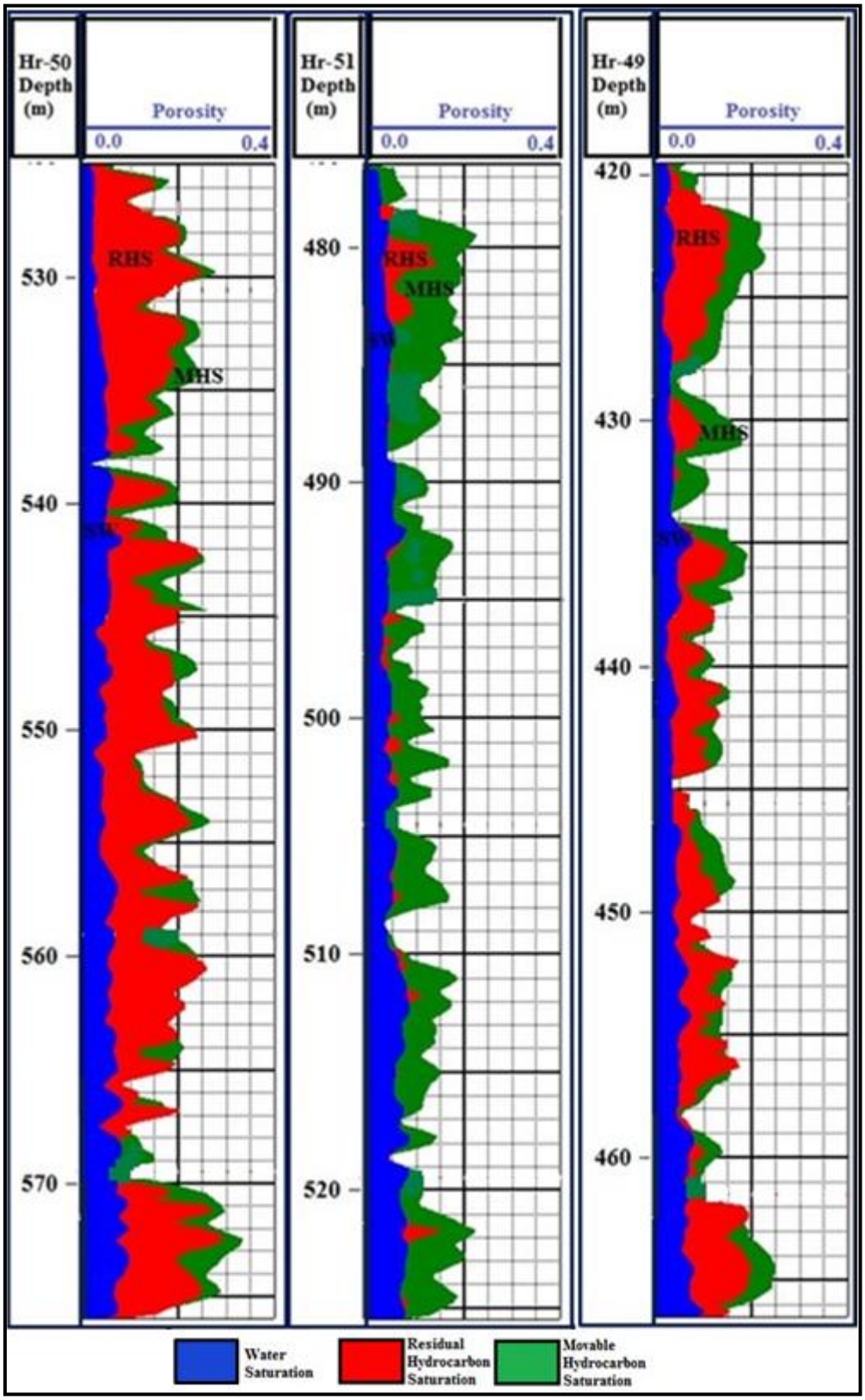

Figure 14. Water saturation and Hydrocarbon saturation (Residual and Movable) with regard to porosity for the studied Jeribe Formation in wells Hr-50, Hr-51, and Hr-49.

As concluded previously, the hydrocarbons in the Jeribe Formation in well Hr-50 are most likely to be oil and hens of higher viscosity than the hydrocarbons in wells Hr-51 and Hr-49, which are expected to be gas. Accordingly, a higher ratio of the hydrocarbons is expected to remain as residual in the rock.

In this study, no wettability tests were done on the rock samples of the Jeribe Formation to find out whether wettability played a role in increasing the ratio of residual hydrocarbons in the formation in well Hr-50.

It's important to mention that a high percentage of the reservoired hydrocarbons in the formation in well Hr-51 is moveable, although the least percentage of the secondary porosity was suggested to be in this well. This can be considered an additional clue that the calculated secondary porosities for the Jeribe Formation in wells of the study (Figure 13) are mostly separated vugs or voids that contribute to increasing porosity without enhancing permeability so much.

4.6. Flow Zone Indicators and Hydrocarbon Moveability

Amaefule et al., (1993) claim that the Flow Zone Indicator (FZI) is a unique metric that incorporates the geological traits of the texture and mineralogy to differentiate across various pore geometrical facies (Hydraulic Flow Units). Based on the sorting of the grains and the tortuosity of the routes connecting them, FZI can therefore be used as an indicator of grain size and shape.

The FZI technique was initially presented by Amaefule et al. (1993) in order to more precisely ascertain the relationship between permeability and porosity for a certain rock type.

In order to define the flow in the rock, they suggested a method based on a special parameter that changes inversely with tortuosity, shape factor, and grain surface area (Teh et al., 2011). The pore shape of the facies is thus divided into flow zones by the FZI value. A high FZI value indicates that the rock has a lower shape factor and coarse, well-sorted grains. Likewise, a low FZI score suggests that the components of the rock are poorly sorted and fine-grained.

The value of FZI for any interval depends mainly on the measured Reservoir Quality Index (RQI) and the Normalized Porosity Index (Øz) which both can be obtained from the effective porosity (Øe) and permeability (k) of the interval as shown in Equations 11 - 13.

$$RQI = 0.0314\,(\frac{K}{\emptyset e})^{1/2} \tag{11}$$

$$\emptyset z = \frac{\emptyset \mathrm{e}}{1 - \emptyset \mathrm{e}} \tag{12}$$

$$FZI = \frac{\text{RQI}}{\text{Øz}} \tag{13}$$

Where: RQI: Reservoir Quality Index; K: Permeability in mD; Øe: Effective porosity in fraction; Øz: Normalized Porosity Index; FZI: Flow Zone Indicator in µm.

The S-shaped curve in normal probability analysis is a useful tool for identifying the various groups of FZI values, which correspond to various HFUs. The distribution and arrangement of the computed FZI values for the Jeribe Formation in the three wells under study are depicted in Figure 15. What sets one group of FZI values apart from the others is the slope by which they are grouped. In every well under study, four distinct groups of FZI may be differentiated, as shown in Figure 15.

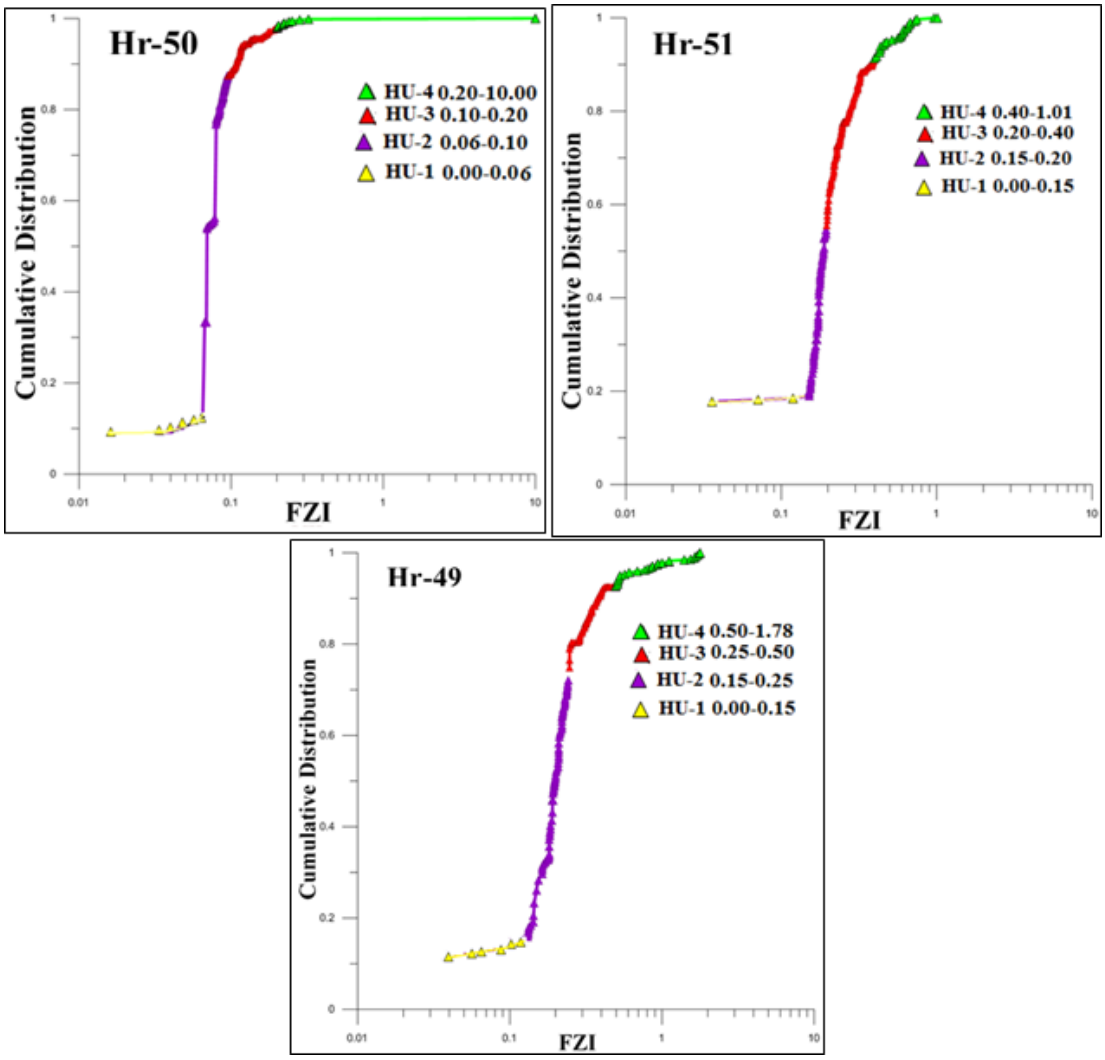

Figure 15. Normal probability analysis for the calculated Flow Zone Indicator values for the Jeribe Formation in each of Hr-50, Hr-51, and Hr-49 wells.

On the other hand, the sample points representing FZI values are dispersed in groups with varied unit slopes when the RQI values are plotted against Øz on a log-log paper (Figure 16). Every

set of points exhibiting a characteristic unit slope denotes a separate HFU. Internal consistency and predictability distinguish each hydraulic flow unit (HFU) from the characteristics of other rock volumes. HFUs are sections of the reservoir rock where the fluid flow is influenced by certain geological and petrophysical factors (Thomas, 2002).

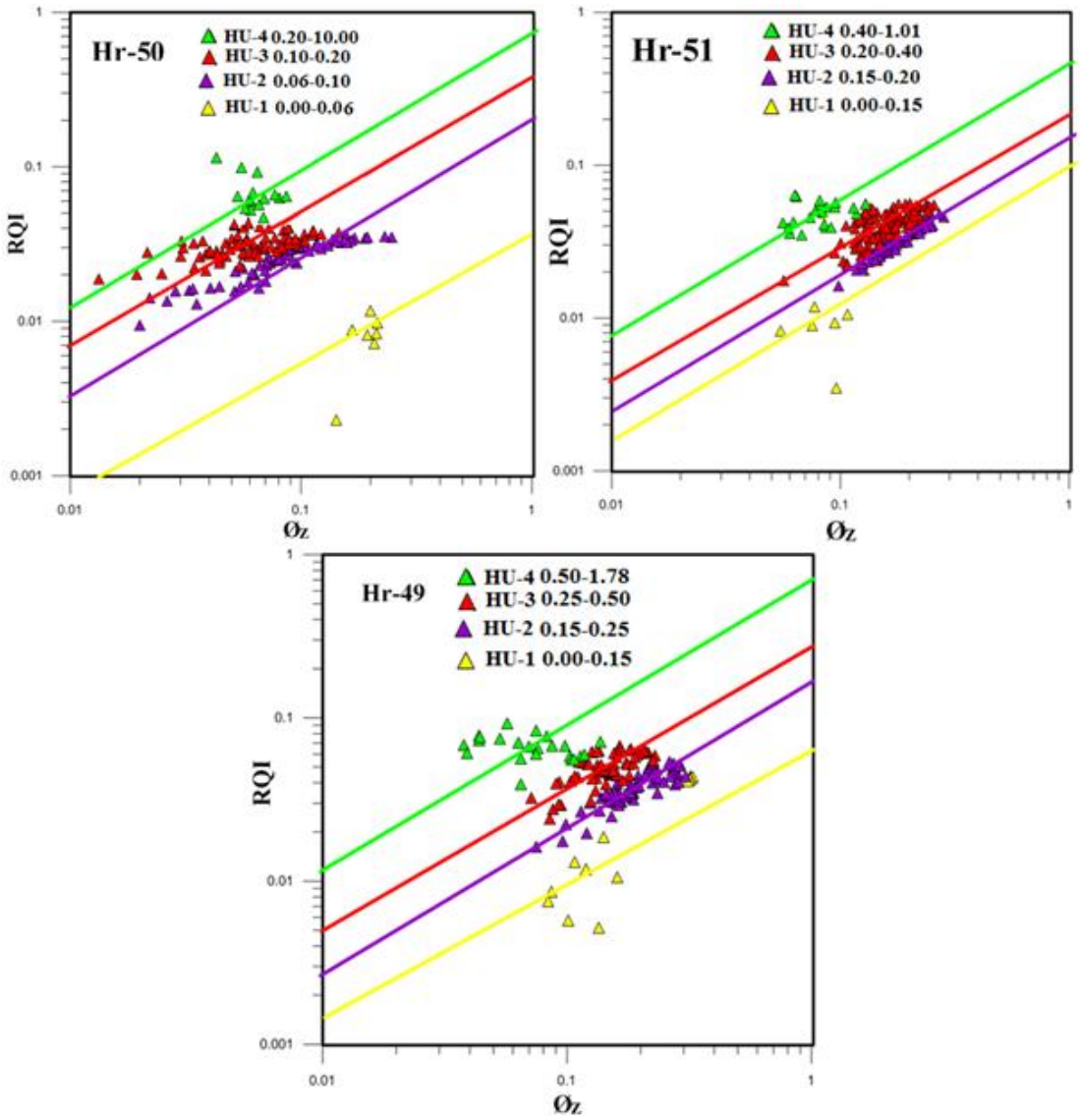

Figure 16. Four unique FZI range values were found in the wells of HR-50, HR-51, and HR-49 that were investigated based on the RQI-Θz connection for the Jeribe Formation.

The names of the HFU are used to represent the FZI groups in Table 6, which also includes the average value for each of the notable FZI groups for the Jeribe Formation in the wells under study as well as their range values and the description of the reservoir rock types (RRT) as suggested by Fea et al. (2022).

The distribution of the RQI versus Øz sample points (Figure 16), which generally have low values, indicates no effective contribution of microfractures in the flow of the fluids (Sadooni,

2004). Moreover, the average values of the RQI and FZI for the identified hydraulic flow units of the Jeribe Formation are, according to Fea et al. (2022), generally indicating a tight reservoir rock type, with only one hydraulic unit (UF-4) in well Hr-49, which showed a poor reservoir type, and another one (HF-4) in well Hr-50, which showed a poor to fair reservoir rock type.

Table 6. Ranges and average FZI values for the hydraulic units of the Jeribe Formation in the studied wells, and their RRT description according to Fea et al. (2022).

Wells	Hydraulic Flow Units	FZI Ranges	Average FZI	Reservoir Rock Type (RRT)
Hr-50	HU-1	0.00 – 0.06	0.0079	Tight
	HU-2	0.06 – 0.10	0.0885	Tight
	HU-3	0.10 – 0.20	0.14	Tight
	HU-4	0.20 – 10.00	5.00	Poor-Fiar
Hr-51	HU-1	0.00 – 0.15	0.06	Tight
	HU-2	0.15 – 0.20	0.18	Tight
	HU-3	0.20 – 0.40	0.28	Tight
	HU-4	0.40 – 1.01	0.60	Tight
Hr-49	HU-1	0.00 – 0.15	0.042	Tight
	HU-2	0.15 – 0.25	0.201	Tight
	HU-3	0.25 – 0.50	0.38	Tight
	HU-4	0.50 – 1.78	1.19	Poor

According to Asquith & Krygowski, (2004); The flushed zone's water saturation (Sxo) can be utilized as a gauge for the moveability of hydrocarbons. For instance, if Sxo is significantly greater than Sw, the invasive drilling fluids (Rmf) have most likely pushed or flushed away the hydrocarbons in the flushed zone from the zone closest to the borehole.

The identification of hydrocarbons from the differential in water saturations in the flushed zone (Sxo) and the uninvaded zone (Sw) is referred to as the ratio technique.

Equation 14 is obtained by dividing the equation of Sw calculation (Equation 7) by the equation of Sxo calculation (Equation 8).

$$Sw/Sxo = [(\frac{Rxo}{Rt})/(\frac{Rmf}{Rw})^{1/n} \quad (14)$$

Regardless of whether hydrocarbons are present in a formation or not, if the ratio Sw/Sxo (also called the Moveable Hydrocarbon Index, or MHI) is equal to or greater than 1.0, then hydrocarbons were not moved during the invasion.

Moveable hydrocarbons are indicated whenever the ratio Sw/Sxo is less than 0.6 for carbonates and less than 0.7 for sandstones (Schlumberger, 1972).

MHI values have been calculated for the Jeribe Formation in wells of the study, as shown in Figure 17. The 0.6 number is utilized as a cutoff value to distinguish between zones containing moveable hydrocarbons and non-movable hydrocarbon zones (or zones with no hydrocarbon content), as the examined Jeribe Formation is formed of carbonate lithology. Most of the zones

with moveable hydrocarbons exist in the upper part of the formation, with well Hr-50 having the lowest number of moveable hydrocarbon-bearing zones and the least efficient hydrocarbon moveability.

Although the Jeribe Formation in the wells of the study, especially in well Hr-51, has a lot of moveable hydrocarbon zones, the formation still shows no great efficiency for flow and production, as the average calculated low RQI and FZI values indicate a tight reservoir rock type for the formation.

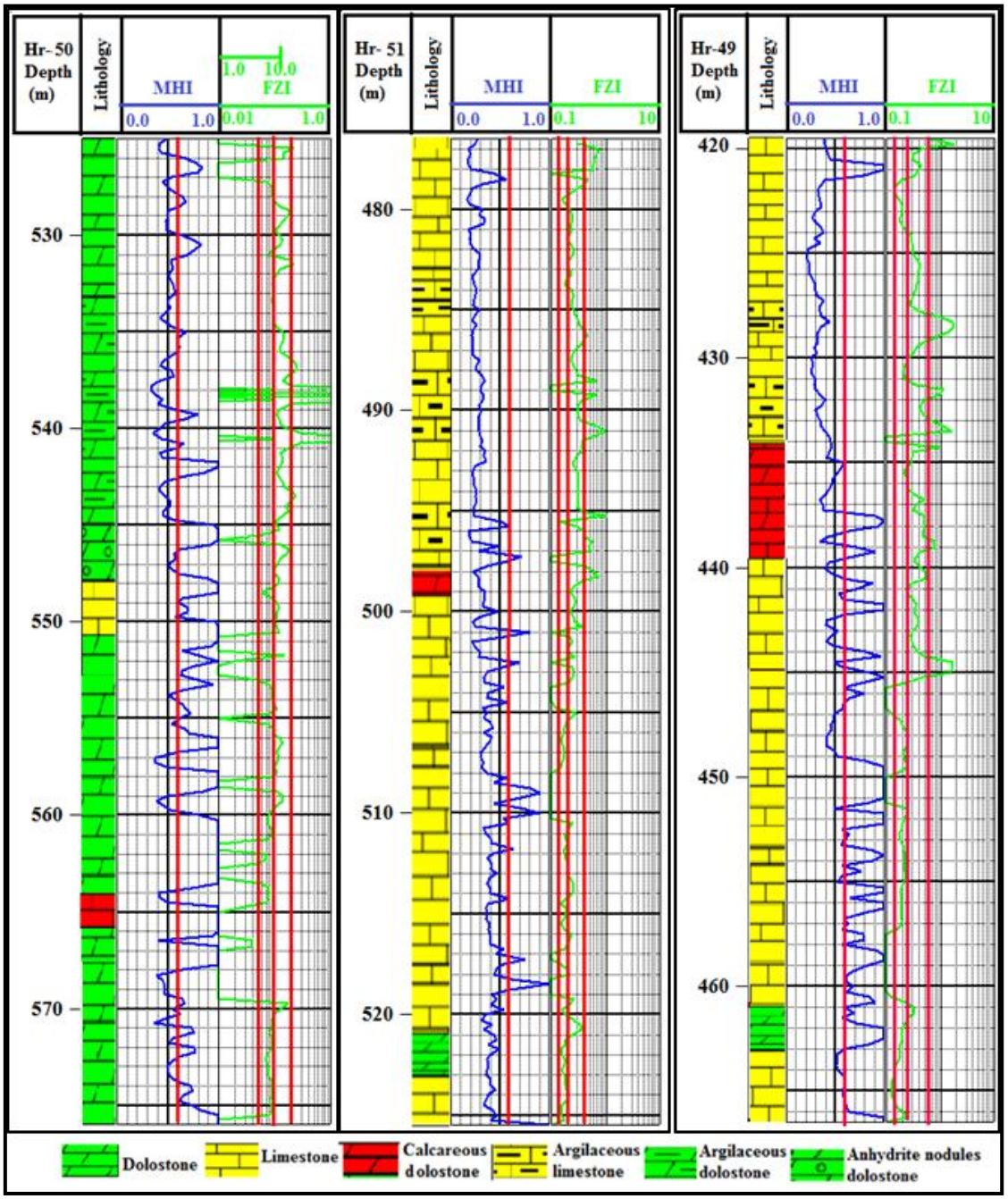

Figure 17. Comparison between the calculated MHI and FZI for the Jeribe Formation in the studied wells of Hr-50, Hr-51, and Hr-49.

5. Conclusions

Based on the microfacies and wireline log analysis done for the Jeribe Formation in the three wells of Hr-50, Hr-51, and Hr-49 located at the Allas Dome of the Hamrin Oilfield, it was concluded that the variations in the recorded data of the wireline logs of the formation in well Hr-50 toward locations of wells Hr-51 and Hr-49 northwest are related to both lithology variations and fluid content within the pore spaces of the formation.

The lithology of the Jeribe Formation at the location of well Hr-50 is more dolostone with more common grainstone microfacies and becomes of dominant limestone lithology and higher wackestone and packstone microfacies content towards the other two wells.

The formation in well Hr-50 is about 18.2% average shale content and about 18.8% average porosity, and in well Hr-51 the average shale content in the formation is about 16.21% and the average porosity is about 12.37%, whereas in well Hr-49 the average shale content and average porosity are 18% and 12.73%, respectively. The shale of the formation in well Hr-50 has dispersed, laminated, and structural modes of distribution, whereas dispersed shale is almost the only way by which the shale is distributed in the Jeribe Formation in the other two wells.

Separated vugs, voids, and molds appear to represent the secondary porosity in the formation, with the highest percentage in well Hr-50 (average 3.1%). The Jeribe Formation in wells Hr-51 and Hr-49 has predominantly gas as a reservoired hydrocarbon, while in well Hr-50, oil is more likely to be the reservoired hydrocarbon in the formation with a sizable immovable fraction. The calculated RQI and FZI values for the Jeribe Formation in the three wells of the study indicate a tight reservoir rock type for the formation.

Acknowledgments

The authors would like to express their deepest appreciation to the North Oil Company (NOC) in Kirkuk, Iraq, for providing the rock samples and log data used in this study.

References

Abdulrahman, S. S., Alkubaisi, M. S., & Al-Shara'a, G. H. (2020). Formation Evaluation for Jeribe Formation in the Jaria Pika Gas Field. *The Iraqi Geological Journal*, 83–93. https://doi.org/10.46717/igj.53.2F.6Ms-2020-12-29

Akram, R. K., Naqshabandi, S. F., & Sherwani, G. (2023). Integration of petrophysical and geochemical approaches for lower Miocene Euphrates and Jeribe Formations in selected wells in Tawke Oil Field, Northwestern Iraq, Zagros-fold belt. *Journal of African Earth Sciences*, *205*, 105000. https://doi.org/10.1016/j.jafrearsci.2023.105000

Al-Ameri, T. K., & Zumberge, J. (2012). Middle and Upper Jurassic hydrocarbon potential of the Zagros Fold Belt, North Iraq. *Marine and Petroleum Geology*, *36*(1), 13–34. https://doi.org/10.1016/j.marpetgeo.2012.04.004

Al-Ameri, T. K., Zumberge, J., & Markarian, Z. M. (2011). Hydrocarbons in the Middle Miocene Jeribe Formation, Dyala Region, NE Iraq. *Journal of Petroleum Geology*, *34*(2), 199–216. https://doi.org/10.1111/j.1747-5457.2011.00501.x

Alatroshe, R. K. h., Yağmurlu, F., & Al-khatabı, A. R. (2018). Petrographical and Petrophysical Features of the Jeribe Formation at the Khabaz Oil Field, Kirkuk, Northern Iraq. *Süleyman Demirel Üniversitesi Fen Bilimleri Enstitüsü Dergisi*, *22*(3), 1283–1295. https://doi.org/10.19113/sdufenbed.503923

Al-Jaff, L. S., & Hamd-Allah, S. M. (2023). Reservoir Characterization of Jeribe and Euphrates Formations in Qaiyarah OilField. *Iraqi Geological Journal*, *56*(2), 204–213. https://doi.org/10.46717/igj.56.2F.13ms-2023-12-19

AL-Sulaiman, F. A., & Aadi Ahmed, T. (2021). Evaluation of Tertiary Reservoir in Hamrin Oil Field, North Iraq. *Edelweiss Chemical Science Journal*, 3–9. https://doi.org/10.33805/2641-7383.123

Amaefule, J. O., Altunbay, M., Tiab, D., Kersey, D. G., & Keelan, D. K. (1993). Enhanced Reservoir Description: Using Core and Log Data to Identify Hydraulic (Flow) Units and Predict Permeability in Uncored Intervals/Wells. *SPE Annual Technical Conference and Exhibition*, SPE-26436-MS. https://doi.org/10.2118/26436-MS

Aqrawi, A. A. M., Goff, J. C., Horbury, A. D., & Sadooni, F. N. (2010). *Petroleum Geology of Iraq*. Scientific press Lt Po box 21, Beaconsfield, Bucks HP9 1NS, UK.

Asquith, G. B., & Gibson, C. R. (2004). Basic well log analysis. In *AAPG methods in exploration series* (2nd ed). American Association of Petroleum Geologists.

Asquith, G. B., & Krygowski, D. (2004). Basic well log analysis. In *Methods in exploration series* (2. ed). AAPG.

Azeez, H. S., Al-Dabaj, Dr. A. A., & Lazim, Dr. S. A.-R. (2020). 3D Petrophysical Model for Mansouriya Gas Field/Jeribe Formation by using Petrel. *Journal of Petroleum Research and Studies*, *10*(1), 36–54. https://doi.org/10.52716/jprs.v10i1.297

Baban, D. H., Abdulla, A. S., & Omar, H. M. (2018). Applications of quick look methods for evaluating the Middle Miocene Jeribe Formation from a selected well in Jambour Oilfield, Kurdistan Region, northern Iraq. *Journal of Petroleum Exploration and Production Technology*, *8*(3), 733–741. https://doi.org/10.1007/s13202-017-0426-z

Baban, D. H., & Ahmed, M. M. (2022). Characterization of the Carbonate Reservoir Unit A of the Upper Triassic Kurra Chine Formation in the well SH-4, Shaikan Oilfield, Iraqi Kurdistan Region, Using Wireline Log Data. *Tikrit Journal of Pure Science*, *26*(2), 71–87. https://doi.org/10.25130/tjps.v26i2.122

Baban, D. H., Barzanji, S. S. S., & Ahmed, M. M. (2023). Evaluation of the Shale Impact on Reservoir Characterization, the Jeribe Carbonate Reservoir in an Oilfield Northern Iraq as a Case Study. *The Iraqi Geological Journal*, 185–207. https://doi.org/10.46717/igj.56.2E.14ms-2023-11-19

Baban, D. H., Qadir, F., & Mohammed, A. (2020). Reservoir Rock Properties of the Upper Cretaceous Shiranish Formation in Taq Taq Oilfield, Iraqi Kurdistan Region. *Journal of Zankoy Sulaimani - Part A*, *22*(1), 363–388. https://doi.org/10.17656/jzs.10799

Baban, D., & Hussein, H. S. (2016). Characterization of the Tertiary reservoir in Khabbaz Oil Field, Kirkuk area, Northern Iraq. *Arabian Journal of Geosciences*, *9*(3), 237. https://doi.org/10.1007/s12517-015-2272-y

Barzanji, S. S., Baban, D. H., & Ahmed, M. M. (2023). Moveability and Nature of the Reservoir Hydrocarbons in the Lower Miocene Jeribe Formation in X-Oilfield, Northern Iraq. *The Iraqi Geological Journal*, 80–92. https://doi.org/10.46717/igj.56.1F.6ms-2023-6-14

Bellen, R. C. Van, Dunnington, H. V., Wetzel, R., & Morton, D. M. (1959). *Lexique stratigraphique international. Asie, Fascicule 10a, Iraq: Vol. Volume 10a*. Centre National de la Recherche Scientifique (CNRS), Paris.

Buday, T. (1980). *Stratigraphy and Paleontology" in The Regional Geology of Iraq: Vol. I.* Dar Al-Kutub Publishing House.

Deabl, R. A., Ramadhan, A. A., & Aldabaj, A. A. (2020). Permeability Determination of Tertiary Reservoir/Ajeel Oil Field. *Journal of Engineering*, *26*(7), 206–216. https://doi.org/10.31026/j.eng.2020.07.14

Deabl, R., Ramadhan, A., & Al-Dabaj, A. (2021). Evaluation of Petrophysical Properties Interpretations from Log Interpretation for Tertiary Reservoir /Ajeel Field. *Iraqi Journal of Oil and Gas Research (IJOGR)*, *1*(1), 28–44. https://doi.org/10.55699/ijogr.2021.0101.1009

Ellis, D. V., & Singer, J. M. (2007). *Well Logging for Earth Scientists* (2 edition). Springer Netherlands. http://link.springer.com/10.1007/978-1-4020-4602-5

Fadhil T., D. (2013). *Sedimentological and Reservoir Characterization for Jeribe Formation at Allas Dome/North Hamrin Oil Field.*

Faidhllah, D. K., & Hamd-Allah, S. M. (2023). Building of a Static Model for Jeribe Formation in Jambour Oil Field. *The Iraqi Geological Journal*, 188–197. https://doi.org/10.46717/igj.56.2A.14ms-2023-7-23

Fea, I., Abioui, M., Nabawy, B. S., Jain, S., Bruno, D. Z., Kassem, A. A., & Benssaou, M. (2022). Reservoir quality discrimination of the Albian-Cenomanian reservoir sequences in the Ivorian basin: a lithological and petrophysical study. *Geomechanics and Geophysics for Geo-Energy and Geo-Resources*, *8*(1), 1. https://doi.org/10.1007/s40948-021-00297-8

Gharib, A. F., & Özkan, A. M. (2022). Reservoir Evaluation of the Tertiary Succession in Selected Wells at Ajeel Oilfield, Northern Mesopotamian Basin, NE Iraq. *Arabian Journal of Geosciences*, *15*(12), 1147. https://doi.org/10.1007/s12517-022-10419-5

Ghorab, M., Ramadan, A. M., & Nouh, A. Z. (2008). The relation between shale origin (source or nonsource) and its type for Abu Roash Formation at Wadi-El Naturn area, south of Western Desert, Egypt. *Australian Journal of Basic Applied Sciences*, *2*(3), 360–371.

Hussein, D., Collier, R., Lawrence, J. A., Rashid, F., Glover, P. W. J., Lorinczi, P., & Baban, D. H. (2017). Stratigraphic correlation and paleoenvironmental analysis of the hydrocarbon-bearing Early Miocene Euphrates and Jeribe formations in the Zagros folded-thrust belt. *Arabian Journal of Geosciences*, *10*(24), 543. https://doi.org/10.1007/s12517-017-3342-0

Hussein, D., Rashid, F., Lawrence, J. A., Glover, P. W. J., & Lorinczi, P. (2022). Influence of fractures on the reservoir quality of Lower Miocene carbonates in Northern Iraq. *Arabian Journal of Geosciences*, *15*(1), 63. https://doi.org/10.1007/s12517-021-09345-9

Ibrahim, D. M. (2008). *Sedimentology and reservoir characteristics of Jeribe Formation (Middle Miocene) in Tawke Oil Field, Zakho, Kurdistan Region - Iraq*.

INOC. (1994). *The annual report of the reservoirs for the year 1993*.

Jassim, S. Z., & Buday, T. (2006). Chapter 14: Latest Eocene-Recent Megasequenece AP11 : In S. Z. Jassim & T. Buday (Eds.), *Geology of Iraq* (1. ed, pp. 341–352). Dolin, s.r.o., distributed by the Geological Society of London.

Kurniawan, F., & Kurniawan, B. (1996). Shaly sand interpretation using CEC-dependent petrophysical Shaly sand interpretation using CEC-dependent petrophysical parameters shaly sand interpretation using cec-dependent petrophysical parameters. In *M.S. in Petroleum Engineering*. https://repository.lsu.edu/gradschool_dissertations

Larionov, W. W. (1969). *Radiometrija Skwaschin*.

Mahdi, A. Q. (2015). *Source rock evaluation of the Najmah, Chia Gara, and Balambo formations and related crude oils, Northwestern Zagros Basin, Northern Iraq.*

Moradi, S., Moeini, M., Ghassem al-Askari, M. K., & Mahvelati, E. H. (2016). Determination of Shale Volume and Distribution Patterns and Effective Porosity from Well Log Data Based On Cross-Plot Approach for A Shaly Carbonate Gas Reservoir. *IOP Conference Series: Earth and Environmental Science*, *44*, 042002. https://doi.org/10.1088/1755-1315/44/4/042002

Qader, F. M., & Ali, S. M. (2022). Reservoir Characteristics of the Lower Miocene Carbonate Formations in Kor Mor Gasfield, Kirkuk Area, NE Iraq. *Tikrit Journal of Pure Science*, *27*(3), 43–52. https://doi.org/10.25130/tjps.v27i3.52

Rider, M. (2002). The Geological Interpretation of Well Logs. *Aberdeen and Sutherland: French Consulting Ltd., 2nd ed.*

Sadooni, F. N. (2004). Stratigraphy, Depositional Setting and Reservoir Characteristics of Turonian - Campanian Carbonates in Central Iraq. *Journal of Petroleum Geology*, *27*(4), 357–371. https://doi.org/10.1111/j.1747-5457.2004.tb00063.x

Saxena, K., Tyag, A., Klimentos, T., Morriss, C., & Mathew, A. (2006). *Evaluating Deepwater Thin-Bedded Reservoirs with the RT Scanner*. *20*.

Schlumberger. (1972). *Log Interpretation / Charts:* (Vol. 1). Schlumberger Well Services Inc.,.

Schlumberger. (1989). *Log Interpretation Principles/Applications*. Schlumberger Educational Services.

Sharland, P. R., Archer, R., Casey, D. M., Davies R. B., Hall, S. H., Heward, A. P., Horbury, A. D., & Simmons, M. D. (2001). Arabian Plate Sequence Stratigraphy. In *GeoArabia Special Publication No. 2*. Gulf PetroLink.

Teh, W. J., Willhite, G., Doveton, J., & Tsau, J. (2011). Improved Predictions of Porosity from Microresistivity Logs in a Mature Field through Incorporation of Pore Typing. *SPE Eastern Regional Meeting*, SPE-149506-MS. https://doi.org/10.2118/149506-MS

Thomas, B. H. (2002). *Flow unit prediction with limited permeability data using artificial neural network analysis*. https://researchrepository.wvu.edu/etd/2431

Thomas, E. C., & Stieber, S. J. (1975). The distribution of shale in sandstones and its effect upon porosity. *New York, USA.*

Tiab, D., & Donaldson, E. C. (2012). *Petrophysics: theory and practice of measuring reservoir rock and fluid transport properties* (3rd ed). Gulf Professional Pub.

Visser, J. (1998). *Extensive hydraulic fracturing of (saturated) porous materials.*

Yang, L. (2015). *A Petrophysical Evaluation of the Trenton-Black River Formation of the Michigan Basin* [Michigan Technological University]. https://doi.org/10.37099/mtu.dc.etds/914

About the authors

Muhamad B. M. Saeed is a PhD student at the University of Sulaimani, College of Science, Department of Earth Sciences and Petroleum. He also employed the Directorate of Oil and Mineral in Sulaimaniyah, Ministry of Natural Resources in the Kurdistan Region Government. Muhamad is a member of the Kurdistan Geological Society, and he is a member of the Kurdistan Geopark Board. He got his M.Sc. in petroleum geology from the University of Sulaimani. He has nine years of experience as a wellsite geologist in the Miran, Chia Surkh, Sarqala, and KhorMore fields and as an operations engineer in the control room in the Bazian Oil Plant for four years.

e-mail: muhamad.muhamadsaeed@univsul.edu.iq

Dler H. Baban (Ph.D.) is a professor of petroleum geology at the Department of Earth Sciences and Petroleum at the University of Sulaimani. Dler gained his MSc in general geology from the Department of Geology/ University of Baghdad in 1989 and his Ph.D. in petroleum geology in 1996 from the same department. Dler supervised a number of M.Sc. and Ph.D. students in petroleum geology specifications and worked as a consultant for the FAO organization and for a number of foreign oil companies in the southern Kurdistan Region.

e-mail: dler.mohamad@univsul.edu.iq